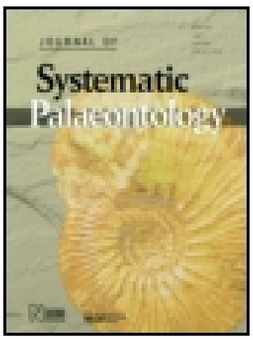

Journal of Systematic Palaeontology

ISSN: 1477-2019 (Print) 1478-0941 (Online) Journal homepage: https://www.tandfonline.com/loi/tjsp20

Anatomy, possible sexual dimorphism, and phylogenetic affinities of a new mylodontine sloth from the late Pleistocene of intertropical Brazil

Cástor Cartelle, Gerardo De Iuliis, Alberto Boscaini & François Pujos

To cite this article: Cástor Cartelle, Gerardo De Iuliis, Alberto Boscaini & François Pujos (2019): Anatomy, possible sexual dimorphism, and phylogenetic affinities of a new mylodontine sloth from the late Pleistocene of intertropical Brazil, Journal of Systematic Palaeontology, DOI: 10.1080/14772019.2019.1574406

To link to this article: https://doi.org/10.1080/14772019.2019.1574406

Published online: 01 Apr 2019.

Journal of Systematic Palaeontology, 2019
http://dx.doi.org/10.1080/14772019.2019.1574406

Taylor & Francis
Taylor & Francis Group

Anatomy, possible sexual dimorphism, and phylogenetic affinities of a new mylodontine sloth from the late Pleistocene of intertropical Brazil

Cástor Cartelle[a]*, Gerardo De Iuliis[b,c], Alberto Boscaini[d] and François Pujos[d]

[a]*Pontifica Universidade Católica de Minas Gerais (PUC Minas), Avenida Dom José Gaspar, 290 Coração Eucarístico, Belo Horizonte, Minas Gerais, Brazil;* [b]*Department of Ecology and Evolutionary Biology, University of Toronto, 25 Harbord Street, Toronto, Ontario M5S 3G5, Canada;* [c]*Section of Palaeobiology, Department of Natural History, Royal Ontario Museum, 100 Queen's Park Crescent, Toronto, Ontario M5S 2C6, Canada;* [d]*Instituto Argentino de Nivología, Glaciología y Ciencias Ambientales (IANIGLA), CCT-CONICET-Mendoza, Avda. Ruiz Leal s/n, Parque Gral. San Martín, 5500 Mendoza, Argentina*

(Received 5 June 2018; accepted 8 January 2019)

Glossotherium phoenesis sp. nov. from the late Pleistocene of intertropical Brazil is described and compared with *Glossotherium robustum* and *Glossotherium tropicorum*. Compared to these two species, the main differences occur in the shape of the nasal region and pterygoids, proportionate narrowing of the skull, length and arrangement of the tooth rows, degree of projection and form of the mandibular symphysis, height at various points along the dentary, and proportions of the radius, among others described. Clear differences in two well-preserved skulls of the new species are interpreted as representing sexual dimorphism, as occurs in other ground sloths such as *Paramylodon* and *Eremotherium*. Other notable features are described for osteoderms and for the ontogenetic developments of the mandible and dentition. The new species *G. phoenesis* appears to be one of the most derived Mylodontidae, sister taxon of *G. tropicorum*, and closely related to *Pleurolestodon*.

http://zoobank.org/urn:lsid:zoobank.org:pub:3F1BAFDB-FC4A-442E-ADFD-692EB2DC7655

Keywords: Xenarthra; *Glossotherium*; new species; sexual dimorphism; osteoderms; evolution

Introduction

Xenarthra may be considered as the most representative clade of Cenozoic South American placental mammals. It includes two groups, the armoured Cingulata (armadillos, pampatheres and glyptodonts) and Pilosa, comprised by the South American anteaters (Vermilingua) and the sloths (Folivora = Phyllophaga = Tardigrada). Four main Folivora clades, generally considered families, are usually recognized: Megalonychidae, Megatheriidae, Mylodontidae and Nothrotheriidae. A fifth, the monogeneric Bradypodidae, includes *Bradypus*, the living three-toed sloth (e.g. see McDonald & De Iuliis 2008; Slater *et al.* 2016) and reflects the consensus that this genus is the sister group to all remaining sloths (but see Buckley *et al.* 2015).

Mylodontids, known from the late Oligocene (e.g. *Octodontotherium* from La Flecha, Argentina; Hoffstetter 1956) to the early Holocene (e.g. *Mylodon* from Ultima Esperanza Cave, Chile; Martin 2018), comprise a clade of large-sized sloths that diversified widely throughout South America, but had a more restricted diversity in North America during the latter part of the Cenozoic (e.g. Saint-André *et al.* 2010). The four mylodontid subgroups usually recognized (traditionally considered subfamilies) are Mylodontinae, Lestodontinae, Urumacotheriinae and Scelidotheriinae, although some authors also recognize Nematheriinae and Octomylodontinae (see Rinderknecht *et al.* 2010 and Saint-André *et al.* 2010 for further details). The first discoveries of Mylodontinae were made by Charles Darwin in Uruguay and Argentina, and were reported on initially by Owen (1839), who erected *Mylodon darwinii* and *Glossotherium* (the latter only as a genus) based on partial cranial remains. Later, Owen (1842) described the nearly complete skeletal remains of a single individual as *Mylodon robustus*. Through a tortuous taxonomic path, the latter has come to be regarded as the type of *Glossotherium robustum*. The taxonomic history of this genus has been hindered not only by incorrect determination of the original type specimen, but also by the multiplication of species based on insufficiently diagnosable remains recovered from various South American countries (McAfee 2009; Pitana *et al.* 2013; De Iuliis *et al.* 2017). For example, in regard to *G. robustum*, Esteban (1996) recorded up to 22 synonyms

Corresponding author. Email: fpujos@mendoza-conicet.gov.ar

Published online 01 Apr 2019

for Argentinian remains attributable to the two species *G. robustum* from the Pleistocene and *Glossotherium chapadmalensis* from the Pliocene. McAfee (2009) recognized six synonyms for *G. robustum*, among them *Glossotherium wegneri* from Ecuador, a species that Esteban (1996) considered as belonging to a distinct genus *Oreomylodon wegneri*, and species of *Pseudolestodon* and *Mylodon*. Mones (1986) listed 17 specific epithets assigned to *Glossotherium*. The current report follows Esteban (1996) in recognizing two Pleistocene species of *Glossotherium*: *G. robustum* and *G. tropicorum*. De Iuliis *et al.* (2017) considerably enhanced the previously restricted understanding of the latter. In Mexico, the Pliocene species *Glossotherium garbanii* was named, but this species has also been assigned to *Glossotherium* sp., *G. chapadmalense* and *Paramylodon garbanii* (Montellano-Ballesteros & Carranza-Castañeda 1986; Morgan 2008; Haro *et al.* 2016).

In Brazil, several Miocene mylodontid species have been recorded from the Amazonian state of Acre: *Octodontobradys puruensis*, *Urumacotherium campbelli*, *Pseudoprepotherium venezuelanum*, and several species allied to *Ranculcus* (Negri *et al.* 2010; Pujos *et al.* 2017).

Two biogeographical regions, intertropical and temperate, are distinguished for the Pleistocene of Brazil. The latter includes areas extending south from the present Tropic of Capricorn and encompasses the states of Rio Grande do Sul, Santa Catarina, Paraná and the southern part of the state of São Paulo. The composition of the mylodontid fauna from this area resembles those that occurred in Argentina, Paraguay and Uruguay. In the vast area encompassed by intertropical Brazil, the composition differs. Some taxa of Folivora are common to both regions. For example, the giant megatheriid *Eremotherium laurillardi* is noted from Rio Grande do Sul (Toledo 1986) and the scelidotheriine *Catonyx cuvieri* is noted from Uruguay (Corona *et al.* 2013), but both species have predominantly intertropical records. The giant mylodontid *Lestodon armatus* is predominantly temperate but is recorded from the state of São Paulo (Henriques 1992). By contrast, the following extinct sloths are autochthonous to the Brazilian intertropical region: *Valgipes bucklandi*, *Ocnotherium giganteum*, and *Mylodonopsis ibseni*, among Mylodontidae; the nothrotheriid *Nothrotherium maquinense* and the megalonychids *Aytherium aureum* and *Australonyx aquae* (Cartelle *et al.* 2008, 2009; De Iuliis *et al.* 2009).

Winge (1915) signalled, in the intertropical region, the presence of '*Mylodon robustus*' (=*Glossotherium robustum*) in Lagoa Santa, Minas Gerais State. However, the remains attributed to this species by Winge (1915, pl. 26) belong to the gigantic and poorly known *Ocnotherium giganteum*, with the exception of a cuboid that belongs to a large Megalonychidae (Pujos *et al.*, in prep.). The first correct identification of *G. robustum* in Brazil was by Paula Couto (1953) based on remains from Rio Grande do Sul, from which additional elements were later recovered (Cartelle & Fonseca 1981; Pitana *et al.* 2013). Simpson & Paula Couto (1981) assigned several remains from the Vale do Rio Juruá (Acre) to *G. wegneri*, but this requires confirmation. Abuhid (1991) recorded *Glossotherium* aff. *G. lettsomi* from Bahia state and Cartelle & Hiroka (2005) assigned material from Mato Grosso do Sul state to the same taxon. Later, Pitana *et al.* (2013) regarded Abuhid's material as *Glossotherium* sp. Finally, remains from states of Paraná (Silva & Sedor 2008), Sergipe (Dantas 2009), Ceará (Ximenes *et al.* 2010), Paraiba (Bergqvist *et al.* 1997), Mato Grosso (Vialou *et al.* 1995) and Mato Grosso do Sul (Salles *et al.* 2006) were identified as *Glossotherium* sp. These assignments, except that from Rio Grande do Sul, require review.

Remains from Muaco, Falcón state of Venezuela, were assigned by Bocquentin-Villanueva (1979) and Aguilera Socorro (2006) to *G. tropicorum*. As noted by De Iuliis *et al.* (2017), they appear to be distinct from the *G. tropicorum* material from Ecuador and Peru and are not considered here because the material is under study by our colleague A. D. Rincón (pers. comm. 2016).

Cartelle & Bohórquez (1982) noted the possibility of sexual dimorphism in the tropical megatheriid *E. laurillardi*, particularly in skull morphology and size of long bones. Cartelle & De Iuliis (1995) demonstrated similar differences in the astragalus of the same species (see also Cartelle & De Iuliis 2006). Intraspecific variation may have been a factor in the erection of several doubtful extinct sloths and especially mylodontid species. Indeed, the morphological differences used to try to justify these species may have reflected sexual dimorphism rather than specific distinctions.

Likewise, Esteban (1996) demonstrated, through figures and measurements, appreciable intraspecific variation that may be attributable to sexual dimorphism in *G. robustum*. McAfee (2009) published comparative measurements of skull features of *G. robustum* and *P. harlani* that also show marked intraspecific variation, which may be interpreted as reflecting sexual dimorphism. Finally, in a study of scelidotheriine skulls, Miño-Boilini & Zurita (2015) reported numerous variations that were interpreted as evidence for sexual dimorphism. Several analyses among extant sloths have also supported sexual dimorphism (e.g. Lara-Ruiz & Chiarello 2005; Hautier *et al.* 2014).

Figure 1. Map of eastern South America indicating the Brazilian locality Toca dos Ossos, from which remains of *Glossotherium phoenesis* sp. nov. have been recovered.

This report analyses two nearly complete skulls from the same locality (Fig. 1; Supplemental Appendix 1) that reinforce sexual dimorphism as a possible explanation of skeletal differences within mylodontines, as shown by McDonald (2006) for the North American species *Paramylodon harlani*. Lydekker (1894, p. 79) suggested the presence of sexual dimorphism in his description and analysis of some 25 "more or less nearly complete skulls" of *Mylodon robustus* (= *G. robustum*). In addition to recognizing 15 synonyms, this author emphasized intraspecific variation of the molariform teeth and morphology of the rostrum in postulating sexual dimorphism in this species.

This report describes a new species of *Glossotherium*, providing a diagnosis that differentiates it from other already well-established species of this genus, and considers its phylogenetic affinities. Evidence related to possible sexual dimorphism is evaluated, as is the function of osteoderms present in the new species and in other mylodontine species.

Material and methods

Remains of several individuals are analysed, permitting diagnostic characters to be identified. Notable among them are: MCL 4303, preserving many skeletal elements, including the skull and mandible (Figs 2, 4, 5A, B, D, E), vertebrae and sacrum (Figs 6, 7) and nearly completely the elements of the forelimb and manus (Figs 8, 9), hind limb (Figs 10, 11) and pes (Figs 12, 13); MCL 4027, a nearly complete skull preserving four molariforms and the alveoli of the other teeth (Figs 3A–D, 5C). In addition, some 100 other isolated elements of the new species, also housed in MCL, are included in the analyses and cited within this report (Supplemental Appendix 1).

Direct comparisons were conducted with the other mylodontine species, cited above, recovered from intertropical Brazil, as well as the skull of *G. robustum* from the Brazilian locality of Cerro da Tapera (MNRJ V-3944), figured by Cartelle & Fonseca (1981) and Pitana *et al.* (2013). The pioneering works of Owen (1842) and Lydekker (1894) contributed significantly to our comparisons, as did images of the holotype and a paratype specimen of *G. tropicorum* (MNHN LAR 237 and MNHN LAR 243, respectively) and remains of this species in the ROM, which are more complete than the holotype and paratype and described recently by De Iuliis *et al.* (2017). A succinct description, including measurements, and diagnosis of the new species is provided, and comparisons with other species of *Glossotherium* are included as part of the Discussion. It is clear (as demonstrated below) that the new species belongs to *Glossotherium*, and so our analysis is restricted to comparisons with other described members of this genus, rather than with all other mylodontines from the Pleistocene.

For the purposes of comparison, we recognize two other Pleistocene species of *Glossotherium*, *G. tropicorum* and *G. robustum*, following Esteban's (1996) proposals (as noted in the Introduction, above). De Iuliis *et al.* (2017) tentatively recognized a third species, *Glossotherium wegneri*, but noted that there are problems with its generic assignment. This species has been identified under diverse designations: its original designation as *Mylodon wegneri* (Spillmann 1931); *Glossotherium wegneri* (Hoffstetter 1948, 1949); *Glossotherium* (*Oreomylodon*) *wegneri* (Hoffstetter 1952); *Oreomylodon wegneri* (Dechaseaux 1971; Esteban 1996); and *G. robustum* (McAfee 2009). The latter author did not justify the synonymy with *G. robustum* (see De Iuliis *et al.* 2017 for further discussion), whereas Esteban's (1996, p. 72) decision was accompanied by a diagnosis for the species. In the

current report, the question whether *Oreomylodon* should be accepted as a distinct genus is left aside, because it is clearly different from the other *Glossotherium* species (for the reasons outlined by De Iuliis *et al.* 2017) and is the subject of an ongoing revision of *Oreomylodon* by the authors.

On the basis of the detailed phylogenetic analysis of the sloths performed by Gaudin (2004), we consider the phylogenetic affinities of the new *Glossotherium* from Brazil with other members of Mylodontidae.

The objectives of this study are: (1) describe a new species of *Glossotherium* from the intertropical region of Brazil, based on sufficiently abundant remains as to provide a clear diagnosis and differentiate the new species, principally through comparisons with *G. robustum* and *G. tropicorum*; (2) highlight the intraspecific variation between two skulls of this species, recovered from the same locality, that suggest the existence of sexual dimorphism; (3) note intraspecific variation in other skeletal elements that may also be attributable to sexual dimorphism; (4) suggest possible functions of the osteoderms present in this and other mylodontine species; and (5) determine the phylogenetic affinities of the new *Glossotherium* species.

Institutional abbreviations

FMNH: Field Museum of Natural History, Chicago, IL, USA; **IVIC**: Instituto Venezolano de Investigaciones Científicas, Caracas, Venezuela; **MCL**: Museo de Ciências Naturais da Pontifícia Universidade Católica de Minas Gerais, Belo Horizonte, Brazil; **MNHN**: Museum national d'Histoire naturelle, Paris, France; **MNRJ**: Museu Nacional do Rio de Janeiro, Rio de Janeiro, Brazil; **NHMUK**: Natural History Museum, London, UK.

Other abbreviations

Cf/cf: upper/lower caniniform tooth; **L**: left; **Mf/mf**: upper/lower molariform tooth; **Mc**: metacarpal; **Mt**: metatarsal; **R**: right.

Systematic palaeontology

Xenarthra Cope, 1889
Pilosa Flower, 1883
Folivora Delsuc *et al.*, 2001
Mylodontidae Gill, 1872
Mylodontinae Gill, 1872
Genus ***Glossotherium*** Owen, 1839

Diagnosis (emended from Esteban 1996). Mylodontine possessing a skull particularly wide mediolaterally, just posterior to the postorbital processes of the frontal bones, differentiating it from *Paramylodon*, *Mylodon* and *Lestodon* (only *Oreomylodon* has similar proportions). The suture between the nasal and the frontal is posteriorly convex. Fibula with either contiguous or separate distal articular surfaces. Femur with deep intercondylar sulcus, culminating in a 'V'-shaped articular outline in anterior view.

Glossotherium phoenesis sp. nov.
(Figs 2–13, 14A)

Holotype. MCL 4303 (Figs 2, 4, 5A, B, D, E, 6H–O, 7–10, 11A–E, 12D–F), the remains of a young adult preserving skull and mandible, with teeth, seven thoracic and three caudal vertebrae, 25 complete or fragmented ribs, right and left humeri, right and left radii, left ulna, sacrum, right ischium, right pubis, left femur, right and left tibiae, and left calcaneum.

Paratype. MCL 4027 (Figs 3A–D, 5C), skull recovered from the same locality as the holotype.

Referred material. For a complete list of specimens (which number well over 100 remains) assigned to this species, refer to Supplemental Appendix 1.

Etymology. The specific epithet *phoenesis* (genitive of *phoenyx*, the indestructible mythical bird that rose from its ashes) honours the students, staff and professors of Museu de Ciências Naturais (MCL, Brazil), who, following the fire of 2013 that destroyed the exhibits of this institution's, found the strength and courage to rebuild them.

Type locality and age. Toca dos Ossos, Ouro Branco, Bahia, Brazil. Late Pleistocene.

Distribution. At least part of the intertropical region of Brazil (Minas Gerais and Bahia States).

Diagnosis. Dorsal skull margin, in lateral view, gently convex over frontoparietal region, becoming shallowly concave at anterior end of frontal, and nearly rectilinear over rostrum. In *G. robustum* nasal region more convex and in *G. tropicorum* both convexity and concavity more pronounced. Narial opening internally taller than wide; nasal does not extend as far anteriorly as maxilla, in contrast to the condition in *G. robustum*. Short predental region, more so than in *G. tropicorum*. Width at pre- and postorbital constrictions very similar. As in *G. robustum*, width of the mastoid region greater than across parietals, whereas in *G. tropicorum* these dimensions are nearly equivalent. Pterygoids with ventral margin nearly rectilinear and projecting little ventrally, with posterior part of base swollen/expanded;

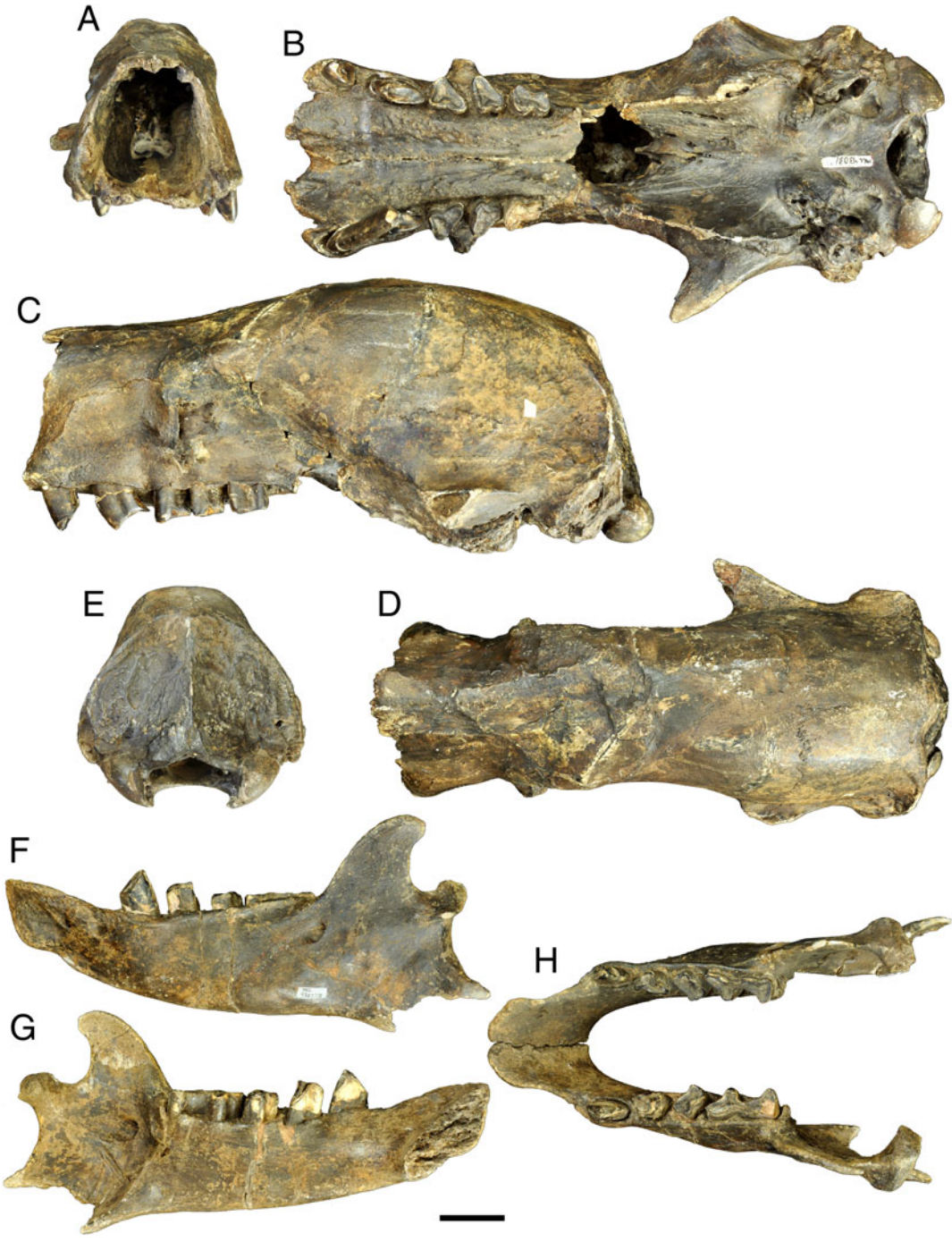

Figure 2. Skull and dentary of *Glossotherium phoenesis* sp. nov. (holotype, MCL 4303). **A–E,** skull in anterior, ventral, lateral, dorsal and posterior views, respectively; **F, G,** left dentary in lateral and medial views, respectively; **H,** mandible in dorsal view. Scale bar = 50 mm.

also, approximately rectilinear in *G. robustum* but not expanded posteriorly; whereas in *G. tropicorum* laterally concave and projecting more prominently ventrally. Occipital ventrally wider than tall, though less than in *G. robustum*; in *G. tropicorum* occipital surface semicircular. Upper tooth row length nearly twice width across the Cf1 alveolar margins; in *G. robustum* and *G. tropicorum*, this proportion is less than 1.5. Height of mandibular body decreases anteriorly more prominently than in *G. robustum* and *G. tropicorum*. Mandibular condyle, in relation to occlusal surfaces of teeth, more dorsal than in *G. tropicorum*. In

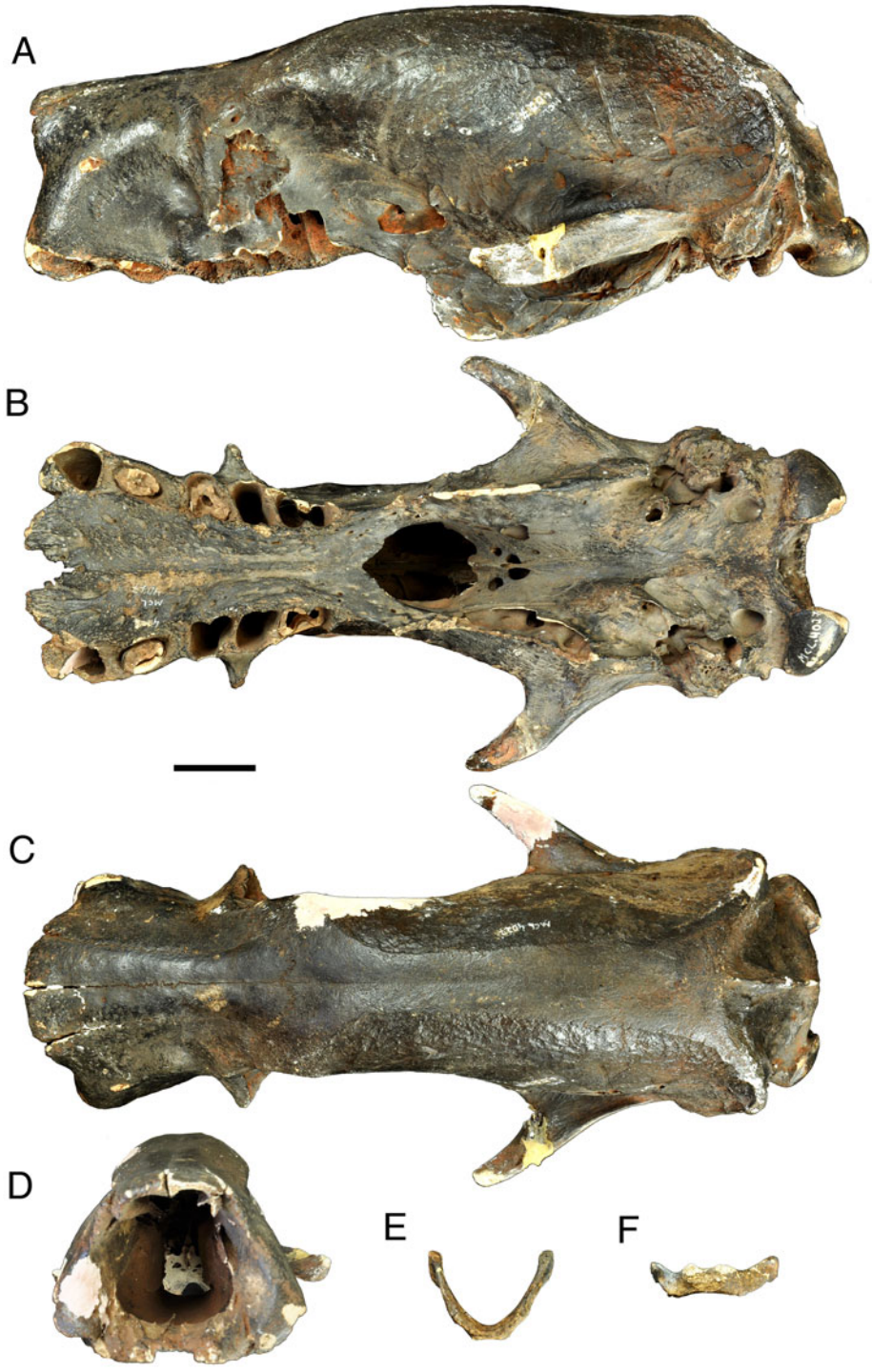

Figure 3. A–D, skull of *Glossotherium phoenesis* sp. nov. (paratype, MCL 4027) in lateral, ventral, dorsal and anterior views, respectively; **E, F,** basihyal of *G. phoenesis* (MCL 4304) in ventral and anterior views, respectively. Scale bar = 50 mm.

consequence, the concavity formed between condyle and posterior margin of coronoid process is smaller than in *G. tropicorum*, whereas concavity outlined by dorsal margin of angular process is markedly more open in *G. phoenesis*, with the angular process being anteroposteriorly narrower and more posteriorly projecting. The dentition is similar to that described for other glossotheres, but Mf1 exhibits mesial wear, which is not observed in the other two Pleistocene glossotheres. Humerus similar to that of *G. robustum* but with less

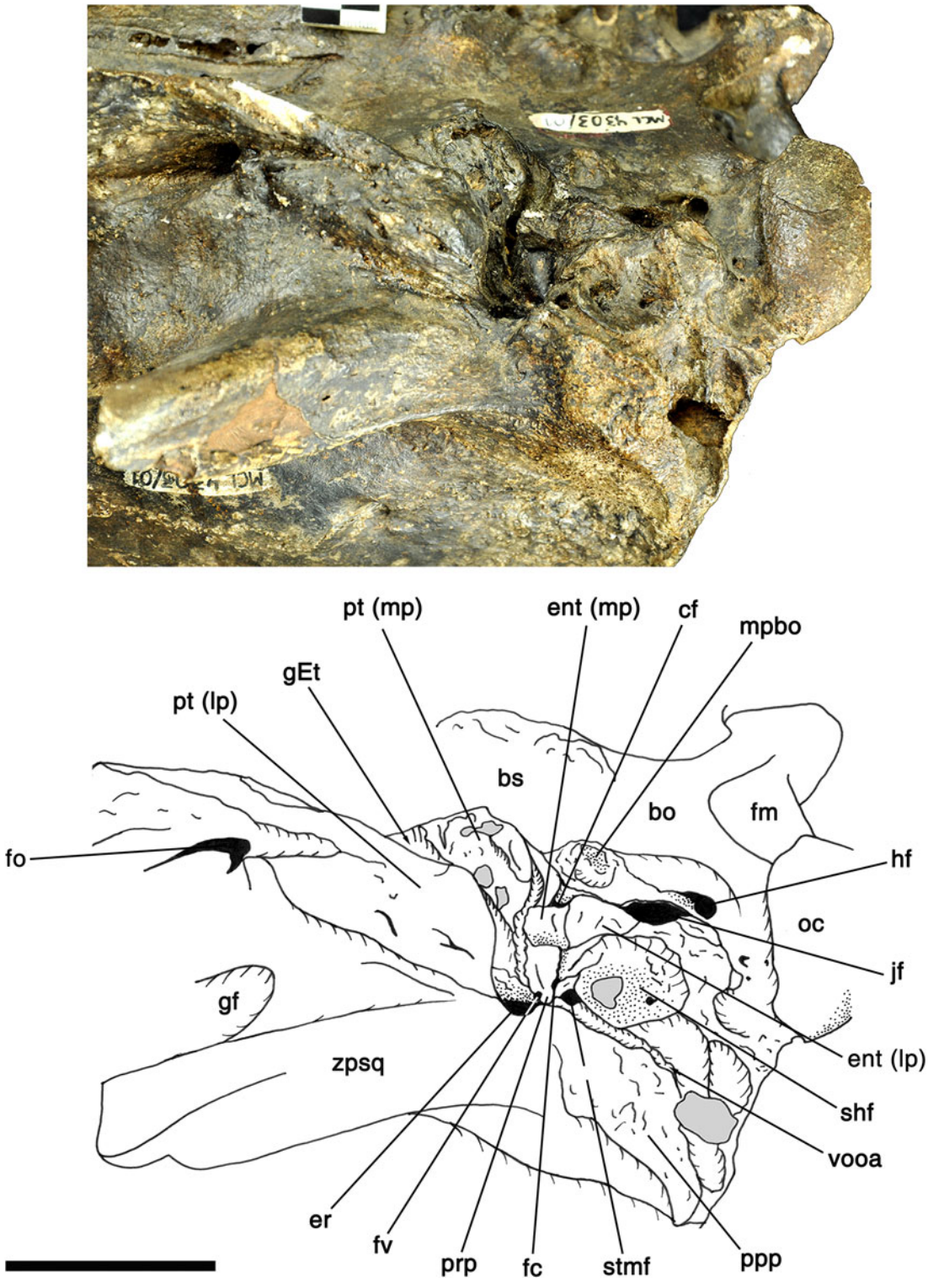

Figure 4. Right ear region of *Glossotherium phoenesis* sp. nov. (holotype, MCL 4303) in lateroventral view. **Abbreviations: bo**, basioccipital; **bs**, basisphenoid; **cf**, carotid foramen; **ent** (**lp**), lateral plate of the entotympanic; **ent** (**mp**), medial plate of the entotympanic; **er**, epitympanic recess; **gEt**, groove for the Eustachian tube; **fc**, fenestra cochleae (= fenestra rotundum); **fm**, foramen magnum; **fo**, foramen ovale; **fv**, fenestra vestibuli (= fenestra ovalis); **gf**, glenoid fossa; **hf**, hypoglossal foramen; **jf**, jugular foramen; **mpbo**, muscular process of the basioccipital; **oc**, occipital condyle; **ppp**, paroccipital process of the petrosal; **prp**, promontorium of the petrosal; **pt** (**lp**), pterygoid (lateral portion); **pt** (**mp**); pterygoid (medial portion); **shf**, stylohyal fossa; **stmf**, stylomastoid foramen; **vooa**, ventral opening of the occipital artery; **zpsq**, zygomatic process of the squamosal. Scale bar = 50 mm.

prominent deltopectoral shelf. Medial margin more strongly concave, entepicondyle more robust and margin of ectepicondyle extending distally more obliquely than in *G. tropicorum*. Proximal half of diaphysis mediolaterally narrower than in *G. tropicorum*. Medial margin curving into ectepicondyle at level of deltopectoral shelf as in *G. robustum*, whereas it extends beyond the shelf in *G. tropicorum*. Ulna gracile and with shorter olecranon than in *G. robustum* and *G. tropicorum*. Fibula with contiguous distal articular surfaces, whereas they are separate in *G. robustum*. The reduced width of the mandibular symphysis at midpoint is autapomorphic for *G. phoenesis*.

Description

Skull

The premaxillae are unknown. The anterior margin of the maxillar palate extends beyond the level of the nasals, and has three notches: a median notch and two smaller lateral notches that articulate with the medial and lateral processes, respectively, of each premaxilla (Figs 2B, 3B). The lateral notch extends posteriorly medial to Cf1, producing a band of bone around the mesial half of this tooth. The maximum length of the palate (excluding the premaxillae) is twice the width between the Cf1s (Supplemental Appendix 1). In the skull of MCL 4303 the molariform tooth rows diverge anteriorly but the Cf1s are set more laterally; indeed, a straight line drawn through the midpoints of the molariform teeth intersects Cf1 lingually (Fig. 2B). In MCL 4027 the molariform tooth rows are more divergent anteriorly, most notably between the Mf1s and Cf1s (Fig. 3B; Supplemental Appendix 2). The posterior palatal margin is approximately 'U'-shaped (Figs 2B, 3B).

The blade-like pterygoids extend nearly vertically. Their ventral margins are nearly perpendicular, with only a very slight lateral concavity. The posterior third of the base of the pterygoid is expanded, reflecting internal pneumatization. The protuberance on the basisphenoid lies medial and posterior to the end of the pterygoid. Both the protuberance and degree of pneumatization are more prominent in MCL 4027 (Fig. 3A, B) than in MCL 4303 (Fig. 2B, C). Posterolateral to the protuberance lies the carotid foramen, separated from the jugular foramen by a portion of the entotympanic (Figs 2C, 3A), which also lies medial to the rugose and circular stylohyal fossa (Fig. 4). The stylomastoid foramen opens along the anteromedial margin of the fossa.

The ectotympanic is not preserved in either of these two skulls, thus revealing the promontory of the petrosal, along with the vestibular and cochlear fenestrae, the latter ventral and posterior to the former (Fig. 4). A foramen, probably for the passage of one of the nerves or blood vessels emerging from the jugular foramen, opens between the carotid and jugular foramina, in the entotympanic itself. The condyloid (or hypoglossal) foramen is smaller than and lies posterior and medial to the jugular foramen (Fig. 4). The foramen for the occipital artery is the most dorsal in this region and opens in a depression between the stylohyal fossa and the paroccipital process of the petrosal. A groove, probably serving to accommodate the Eustachian tube, lies between the lateral and medial portions of the pterygoid as in *G. robustum* (Boscaini *et al.* 2018). The ventral margin of the foramen magnum is semicircular.

The maxillae, projecting beyond the nasals, and the occipital condyles mark the anterior and posterior extent of the skull (Figs 2, 3). The posterior margins of the nasals are convex transversely and form, at the midline, a notch for the frontal, which Esteban (1996) considered characteristic of *Glossotherium*. In MCL 4027 the widths across the pre- and postorbital constrictions are nearly equal (Fig. 3A, C), whereas in MCL 4303 the preorbital constriction is slightly narrower (Fig. 2D; Supplemental Appendix 3). The skull is widest, in both specimens, across the paroccipital processes (=mastoid process of Patterson *et al.* 1992). The rostral width in both specimens at the level of the caniniform teeth is slightly greater than that across the lateral margins of the occipital condyles. In MCL 4027 the rostral width exceeds that across the postorbital (or zygomatic) processes of the frontals (Fig. 3B), whereas the widths are more nearly similar in MCL 4303 (Fig. 2B), a difference attributable to the larger size of the caniniform teeth in the former specimen (Supplemental Appendix 3). In MCL 4303 the temporal lines are barely perceptible and particularly low near the nuchal crests (Fig. 2D). In MCL 4027 they are prominent, curving anteromedially from the nuchal crests, extending forward parallel to one another over their middle course, and then curving anterolaterally towards the postorbital processes of the frontals (Fig. 3C). The lateral margin of the nasal in MCL 4027 is bowed laterally. Width across the nasals at their posterior third is 4.5 cm; more anteriorly, at their widest, the width is 7 cm.

The occipital surface slopes more markedly posteroventrally in MCL 4027 (Fig. 3A). The distance between the transverse planes intersecting the posterior margins of the occipital condyles and the dorsal margin of the nuchal crests is about twice as long in MCL 4027 than in MCL 4303 (Supplemental Appendix 3). Consequently, the maximum skull length is greater in the former (Figs 2, 3).

The dorsal skull profile, from the nuchal margin to the frontoparietal suture, is convex in lateral view,

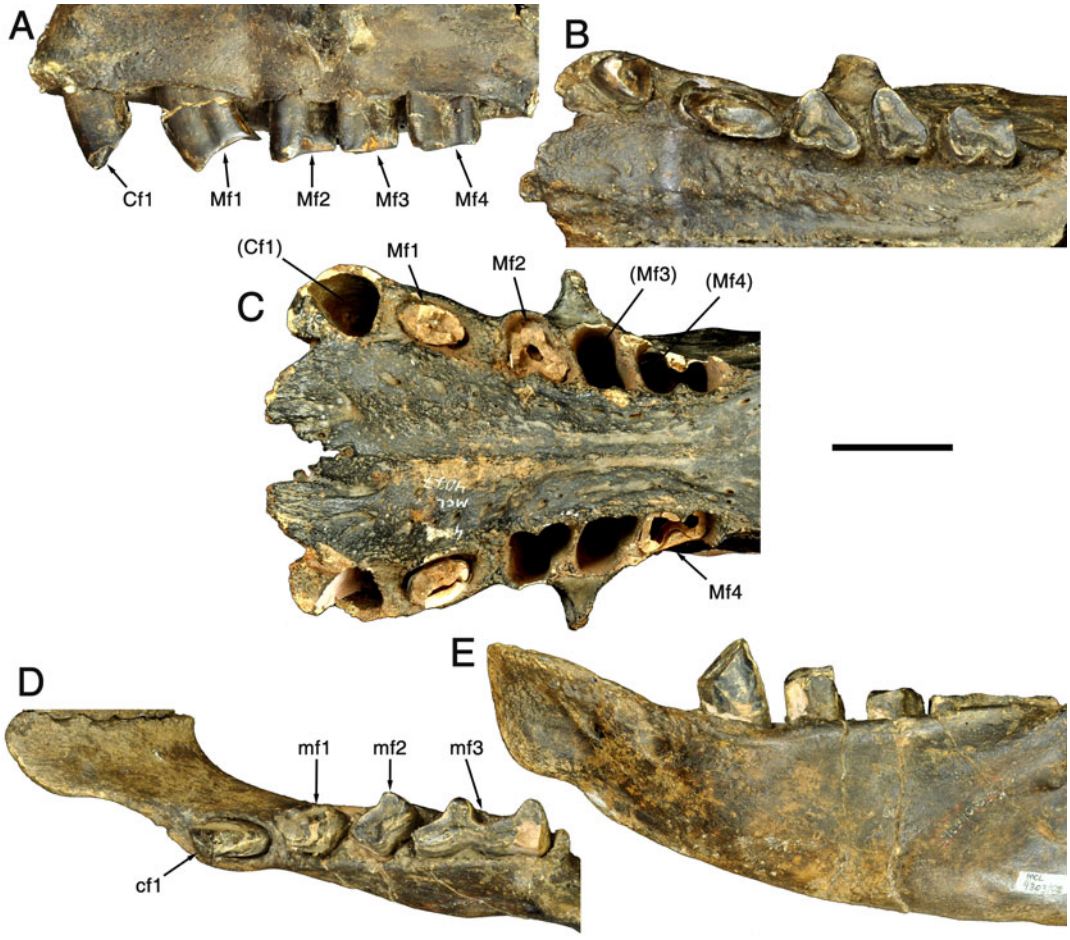

Figure 5. Tooth rows of *Glossotherium phoenesis* sp. nov. **A, B,** upper left tooth row of the holotype (MCL 4303) in lateral and occlusal views, respectively; **C,** upper tooth rows of the paratype (MCL 4027) in occlusal view; **D, E,** left lower tooth row of the holotype (MCL 4303) in occlusal and lateral views, respectively. **Abbreviations: c1**, lower caniniform tooth; **C1**, upper caniniform tooth; **M-**, upper molariform tooth; **m-**, lower molariform tooth. Scale bar = 50 mm.

less prominently so in MCL 4027 than in MCL 4303 (Figs 2C, 3A). Anterior to the suture, the profile descends until reaching the level of the zygomatic process of the maxilla. Over the rostrum, the profile is approximately parallel to the alveolar margin. The greatest height of the skull profile occurs over the anterior part of the pterygoid. In both skulls, the sphenopalatine and optic foramina open within an oval depression on the ventral orbital wall, at the level of the anterior margin of the pterygoid (Figs 2C, 3A). Posterior to the depression lies a fissure or groove that extends towards the common aperture for the sphenorbital fissure and the foramen rotundum. The foramen ovale lies more ventrally and just posteriorly to the midpoint of the pterygoid (Fig. 4). Relative to the zygomatic process, the pterygoid does not project strongly ventrally. Its ventral margin is curved. It is more strongly convex posteriorly in MCL 4303 and anteriorly in MCL 4027. In lateral view, the distance from the foramen ovale to the ventral margin of the pterygoid is nearly equal to the height of the zygomatic process of the squamosal.

The posterior surface of the skull is inclined and bears a median crest extending from the nuchal crest to the margin of the foramen magnum in MCL 4027 (Fig. 3A–C). In MCL 4303 the crest is lower, particularly near the edge of the foramen magnum, and its surface is not as rough (Fig. 2C, D). The dorsal and lateral margins of the occiput circumscribe a semicircular outline, such that the maximum width and height of the occiput are nearly equal (Fig. 2E). The border of the foramen magnum is oval in MCL 4303 but more rounded in MCL 4027 (Fig. 2E; Supplemental Appendix 3). The premaxillae, as noted above, and the vomer are missing. The narial opening widens ventrally in the region of the caniniforms (Figs 2A, 3D). In both MCL 4303 and MCL 4027 the internal heights and widths of the narial

opening are nearly equal, but externally in MCL 4303, which possesses smaller caniniforms, the maximum width is about 25% greater than the height, whereas in MCL 4027 the maximum width is about 33% greater than the height (Supplemental Appendices 2 and 3).

Cf1 and Mf4 occluded with the mesial margin of cf1 and the isthmus and distal lobe of mf3, respectively (Fig. 5A, B). Mf1 occluded against cf1 and mf1; Mf2 with mf1 and mf2; and Mf3 with mf2 and the mesial lobe of mf3. The right and left tooth rows diverge anteriorly less strongly in MCL 4303 (Figs 2B, 5A, B) than in MCL 4027 (Fig. 5C), with divergence most marked between the Cf1s (Supplemental Appendix 3). The latter are sub-circular in section (MCL 4303) or triangular with rounded vertices (MCL 4027). In both specimens Cf1 is curved apicobasally, so that the occlusal surface faces posteriorly, forming an acute angle of about 45° with the mesial part of this tooth. The area of the transverse section of the larger teeth may be twice that of the smaller teeth. Such differences are represented by several isolated adult Cf1s. The different sizes of Cf1 in the two specimens produce widening of the alveoli laterally and are reflected in the differences noted above between the anterior and ventral surfaces of the two skulls (Supplemental Appendix 3). None of the Cf1s bear a flat occlusal surface.

Mf1 is oval or elliptical in section and always exhibits two distinct wear surfaces: a mesial surface caused by occlusion against the distal surface of cf1, and a more flattened surface that occluded against the mesial surface of mf1 (Fig. 5A–C). The tooth is recurved posteriorly (as in other mylodontines; see Gaudin 2004). The remaining three molariforms bear an apicobasal sulcus on their lingual surface; also, a vestibular sulcus is present on Mf4, giving this tooth a figure-of-eight-shaped occlusal outline, in which the distal lobe is larger (Fig. 5B). The vestibular surface of Mf2 and Mf3 are convex, producing a subtriangular outline for these teeth.

Mandible

Eight specimens are available for study. MCL 4008, a right dentary of an adult, does not preserve the symphysis or the angular or coronoid processes, and may belong to the same individual as MCL 4007. The mandible of MCL 4303 (Figs 2F–H, 5D, E), of a young adult, is nearly complete. The other five specimens, MCL 4010, MCL 4011, MCL 4012, MCL 4014 and MCL 4015, represent young or very young individuals (Supplemental Appendix 2). This series, in addition to allowing a better understanding of the morphology of the dentary and lower dentition of the new species, provide valuable information of the ontogeny on this skeletal element.

MCL 4303 is missing only the distal part of its angular process, but the form of this portion may be deduced from its preserved portion (Fig. 2F, G). The dorsal condylar margin lies above the level of the occlusal surfaces of the molariforms. The notch anterior to the condyle is semicircular and narrow, compared to the notch posterior to the condyle. The ascending ramus is short. The anteroposterior length of the condyle is less than the diameter of the notch. The mandibular margin between the condyle and the distal tip of the angular process is widely open, compared to the precondylar notch. The body of the dentary narrows anteriorly to the beginning of the symphysis. At this point, its height is about 15% less than the height of the dentary at the level of mf3 in MCL 4007, and 21% in MCL 4303 (Supplemental Appendix 2). The mylohyoid line and sulcus are clearly evident. The posterolateral opening of the mandibular canal lies at the level of the distal lobe of mf3 anteroposteriorly and at two-thirds the height of the mandibular body dorsoventrally (Fig. 2F). Mental foramina lie at the anterior end of the mandibular body, where it reaches its lowest height. The dorsal margin of the mandibular symphysis lies dorsal to the level of the molariform alveolar margins (Fig. 2F, G). The symphysis extends anteriorly (Fig. 2F–H), and the ventral surface bears a bulge in lateral view.

Ventral to the tooth rows the ventral margin of the dentary is convex. It becomes concave ventral to the level where the body meets the ascending ramus, and becomes convex again posteriorly, with the distal tip of the angular process projecting posterior to the back of the mandibular condyle. The distal tip of the angular process curves medially, though the angular processes themselves diverge posteriorly (Fig. 2H). The condyles are wider transversely than anteroposteriorly and project further medially than laterally. The tooth rows extend nearly parallel to each other (Fig. 2H). The caniniform lies lateral to the molariforms, causing a lateral expansion of the dentary at this point. Along the central part of the mandibular body, its ventral portion projects laterally compared to its dorsal portion, in which the molariforms are implanted. Anterior to the caniniforms the thickness of the dorsal symphyseal margins narrows. The outline of the margin initially forms a lateral concave surface that becomes convex more anteriorly. The maximum transverse width of the symphysis just anterior to cf1 is clearly less than the maximum width between the lingual margins of any two pair of opposite teeth. It is also less than the distance from the mesial surface of the caniniform to the symphyseal anterior margin. The planes passing through the midpoints of the tooth rows from opposite sides are parallel, and pass

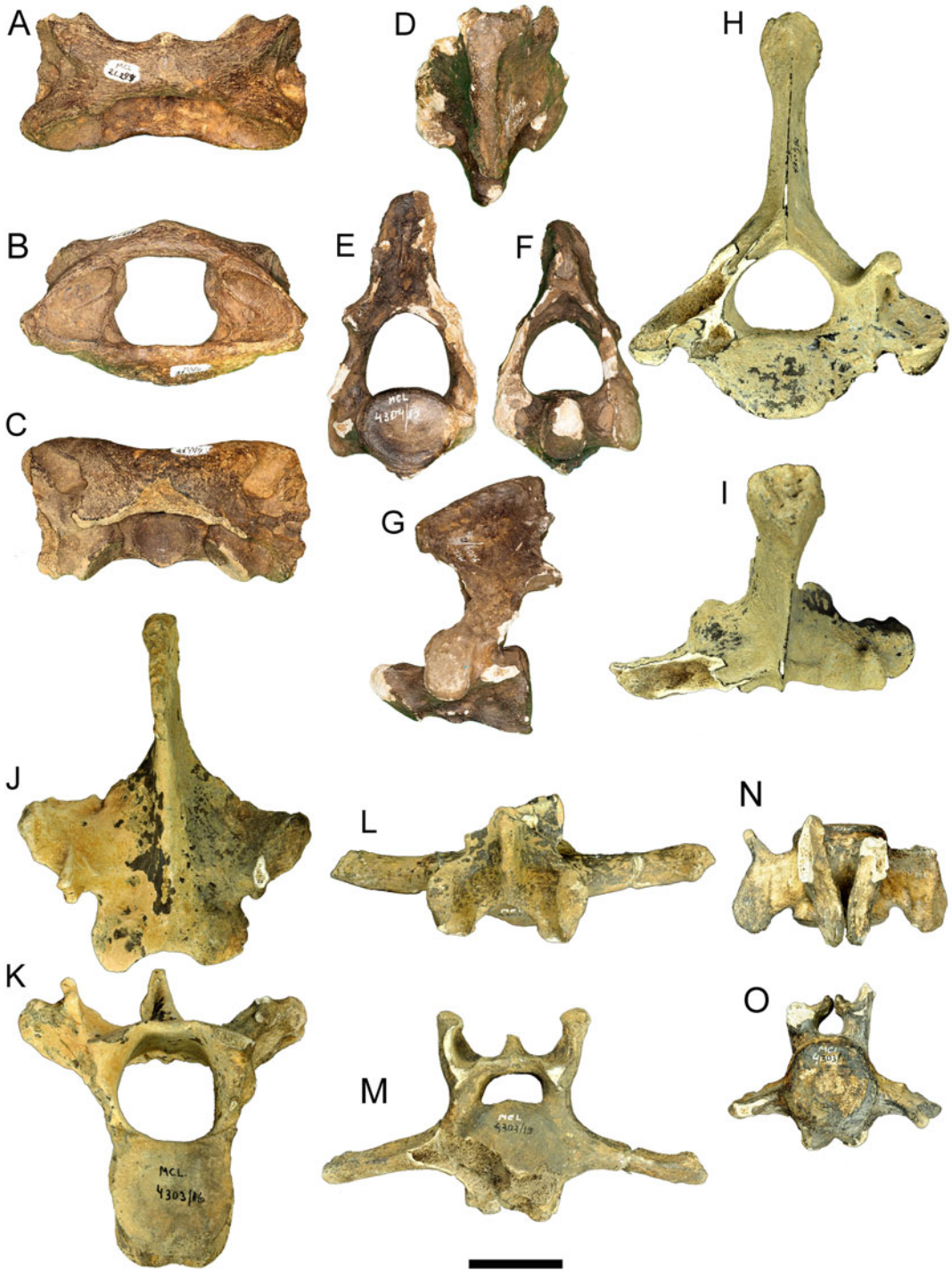

Figure 6. Vertebrae of *Glossotherium phoenesis* sp. nov. (**A–C,** MCL 21244; **D–G,** MCL 4304; **H–O,** holotype, MCL 4303). **A–C,** atlas in dorsal, anterior and ventral views, respectively; **D–G,** axis in dorsal, posterior anterior, and left lateral views, respectively; **H, I,** 1st thoracic vertebra in anterior and dorsal views, respectively; **J, K,** penultimate thoracic vertebra in anterior and dorsal views, respectively; **L–O,** two caudal vertebrae in anterior (**L**, **N**) and dorsal (**M**, **O**) views. Scale bar = 50 mm.

tangentially across the mesial surface of the caniniforms and lateral to the symphyseal margins.

In MCL 4303, cf1 is oval in section, with its major axis oriented mesiodistally; its lingual and vestibular surfaces are flattened and convex, respectively, and its apicobasal axis is nearly rectilinear (Fig. 5D, E). In MCL 4008, which is larger, the lingual surface of cf1 is flat and the mesial, vestibular, and distal surfaces outline

a semicircle. Occlusal wear against Cf1 produced an inclined mesial facet that meets the distal facet of cf1 at an angle of about 45° (Fig. 5E). The distal occlusal surface can be observed in four specimens (MCL 3902, MCL 3946, MCL 4000 and MCL 4001). It is produced by attrition against Mf1. The trilobate mf1 bears apicobasal sulci on its distal, lingual and mesial surfaces, with the latter being less prominent (Fig. 5D). The sulci separate similarly sized mesiolingual, mesiovestibular, and distolingual lobes. The mf2 is rectangular with elongated mesiovestibular and distolingual surfaces, each of which bears an apicobasal sulcus. Its long axis extends vestibulolingually. In mf3, distinct mesial and distal lobes are united by an isthmus (Fig. 5D). The long axis of the larger mesial lobe extends vestibulolingually, and is parallel to the long axis of mf2. The mesial lobe of mf3 is marked by an apicobasal sulcus on its mesial surface. The vestibular margin of the mf3 mesial lobe is longer than its lingual margin. The long axis of the smaller distal lobe of mf3 is also vestibulolingually oriented. The isthmus has a convex vestibular margin and concave lingual margin.

Hyoid apparatus

The thyrohyals and basihyal, preserved in MCL 4304/27, are fused into a 'U'-shaped structure (Fig. 3E). The thyrohyals, forming the greater horns, taper anteriorly. The arch-shaped basihyal is thicker (Fig. 3F). Its anterior margin bears two low processes for articulation with the ceratohyals.

Vertebral column

In the atlas (MCL 21244, Fig. 6A–C), the anterior margin of the dorsal arch is thicker than that of the ventral arch. The articular surfaces for the occipital condyles are markedly concave and narrow transversely. The lateral articular surfaces for the axis are circular and concave, and are obliquely oriented, converging anteriorly. The projected planes of these articular surfaces met anteriorly at an angle of about 90°. The articular surface for the odontoid process, also circular, is larger in area than the lateral axial articular surfaces and extends posteriorly past the margin of the ventral arch of the atlas.

The ventral articular surface of the odontoid process of the axis (MCL 4304, Fig. 6D–G) is oblique, extending anterodorsally, whereas its dorsal, non-articular surface is nearly horizontal. The dorsal margin of the neural spine (or spinous process) inclines posteriorly (Fig. 6G). Its posterior surface projects backward beyond the centrum, whereas its anterior margin lies slightly behind the anterior margins of the lateral atlantal articular surfaces. The latter articular surfaces, occupying the anterolateral part of the centrum, are convex, converge anteromedially, and are oval in outline with their major axes nearly vertical. They are not contiguous with the articular surface on the odontoid process. The transverse processes of the axis are not preserved. The posterior zygapophyses for the 3rd cervical vertebra are borne by pedicles at the vertical midpoint of the posterior axial edge (Fig. 6E). Their margins are the most posteriorly projecting parts of the axis. The ventral width of the vertebral canal is greater than its dorsoventral height. The transverse foramina open at about the dorsoventral midpoint of the articular surfaces for the atlas. The centrum bears a mid-ventral keel.

The neural spine of the first thoracic vertebra (MCL 4303, Fig. 6H, I) narrows anteriorly. A ventrally-facing and concave rib facet lies on the transverse process and a smaller rib facet lies on the centrum at the base of a large pedicle. The former facet served for articulation with the tuberculum of the first rib, whereas the latter facet is a demi facet that articulated with the head, which also articulated with a demi facet on the centrum of the 7th cervical vertebra. Several other thoracic vertebrae are known from MCL 4303 and MCL 4304. In the anterior third of this series, the articular surfaces of the centra range from oval to sub-triangular in outline (Fig. 6J), with the lateral surfaces of the centra converging on a midventral keel. In the more posterior region of the thoracic series, the lateral walls of the centra do not converge as strongly ventrally, and the centra bear two ventral keels. In two thoracic vertebrae from MCL 4304, the right and left pedicles of the neural arch are asymmetric. The neural spines slope posterodorsally (Fig. 6K) and decrease in height and thickness posteriorly. As noted by Engelmann (1985) for all sloths, the transverse processes of the anterior thoracics are larger than those of the posterior thoracics. The transverse processes project posteriorly (Fig. 6K) as well as laterally; the capitular and tubercular facets for the ribs, progressing posteriorly in the thoracic series, go from a more ventral to lateral position, and become single rather than double (i.e. the capitular facets remain).

The ventral surface of the centrum of the last lumbar and first sacral vertebra bears foramina that, according to Hoffstetter (1959), served for passage of the intrarachidean vein. In MCL 4303 the last lumbar is fused to the first of five sacral vertebrae (Fig. 7A, B). Anteriorly in the sacral series, the height of the neural canal is greater than its width. Progressing posteriorly along the series, height diminishes while the width increases. The co-ossified neural processes of the sacrum form a crest of constant width but posteriorly decreasing height (Fig. 7A, B). The ventral surface of the sacrum is transversely

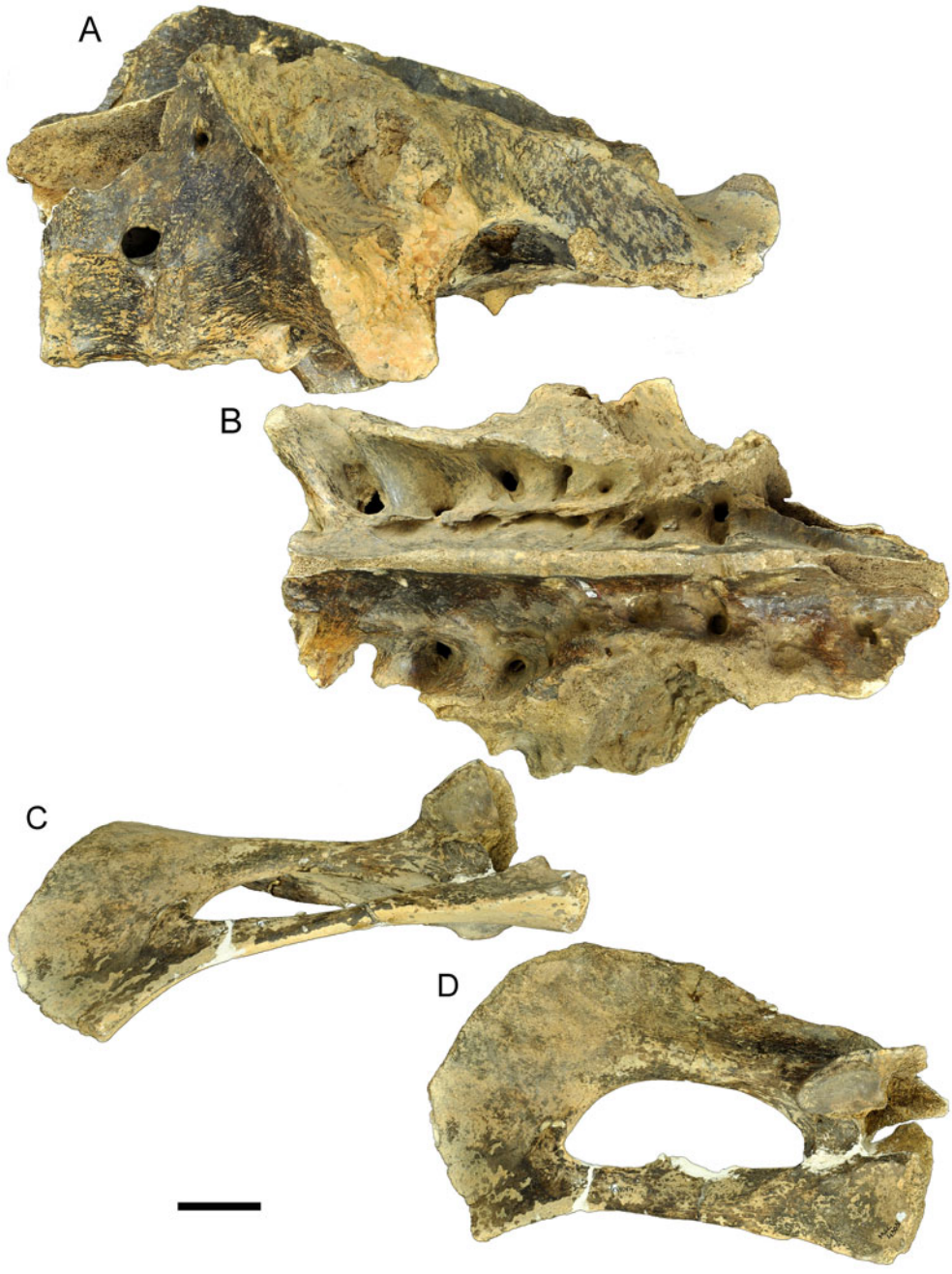

Figure 7. Sacrum and pelvis of *Glossotherium phoenesis* sp. nov. (holotype, MCL 4303). **A, B,** sacrum in left lateral and dorsal views, respectively; **C, D,** right ischium and pubis in anterolateral and medial views, respectively. Scale bar = 50 mm.

concave. Its anterior third is convex longitudinally and becomes concave over the remainder of its length. Five sacral spinal foramina, resulting from fusion of the transverse processes, are present on each side (Fig. 7B). Several preserved caudal vertebrae, mainly from MCL 4303 (Fig. 6L–O) and MCL 4304, are very similar morphologically to those described by Owen (1842) for *G. robustum*.

Appendicular skeleton

Humerus. Available specimens include the right humerus MCL 4303, missing its head, the left humerus of MCL 4303, missing its dorsal ectepicondylar margin (Fig. 8A–E) and the right humerus MCL 4088, missing its proximal third. The head is hemispherical and projects more proximally than the greater tuberosity, which is wider anteriorly than posteriorly (Fig. 8A, C, E). The

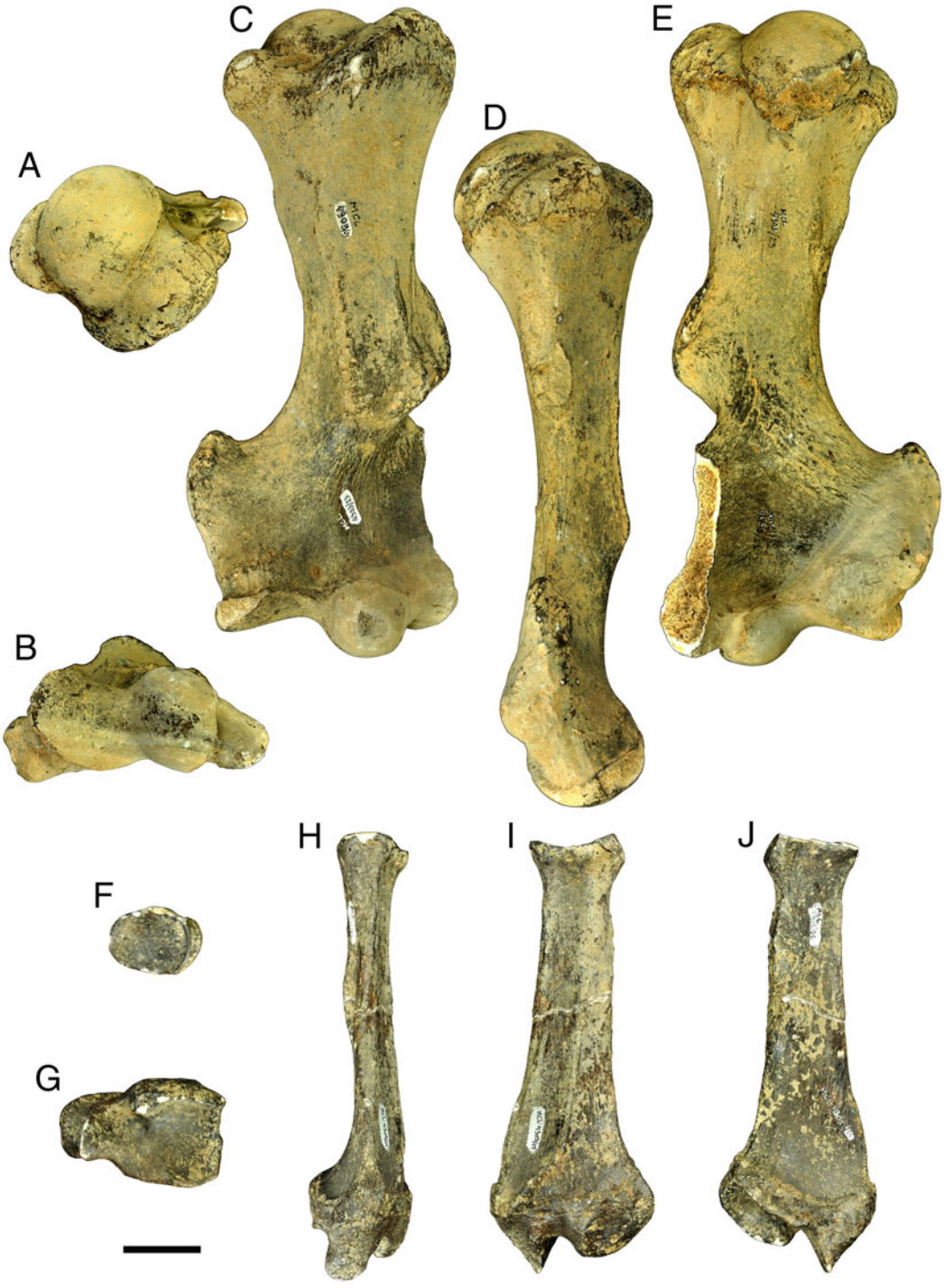

Figure 8. Humerus and radius of *Glossotherium phoenesis* sp. nov. (holotype, MCL 4303). **A–E,** left humerus in proximal, distal, anterior, medial and posterior views, respectively; **F–J,** left radius in proximal, distal, anterior, medial and posterior views, respectively. Scale bar = 50 mm.

rugose deltoid crest projects less laterally than the ectepicondyle, with the margins of the crest and greater trochanter nearly aligned (Fig. 8C). The lateral margin of the ectepicondyle outlines an arch that extends to the capitulum. The proximal part of the entepicondyle is concave, whereas the rest of it is thicker and convex. The capitulum is hemispherical and contiguous with the trochlea (Fig. 8C), which is transversely flat and anteroposteriorly convex. The posterior surface, smoother than the anterior, bears a shallow olecranon fossa (Fig. 8E).

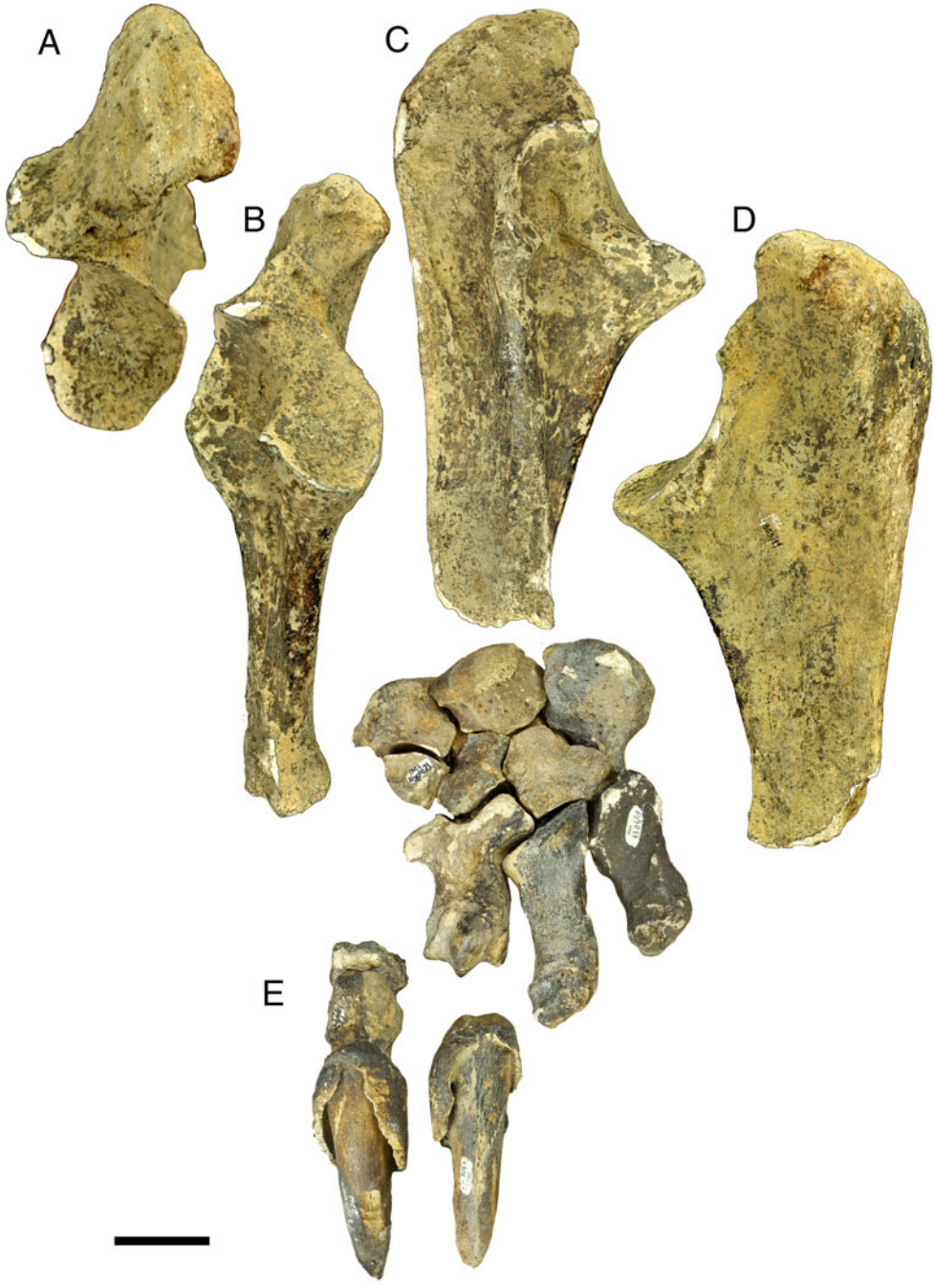

Figure 9. Ulna and manus of *Glossotherium phoenesis* sp. nov. (holotype, MCL 4303). **A–D,** right ulna in proximal, anterior, lateral and medial views, respectively; **E,** left manus in dorsal view. Scale bar = 50 mm.

Radius. Nine radii are available (see Supplemental Appendix 1), three of which are very large. Except for the two from MCL 4303, a young adult with closed epiphyses, the others belong to older individuals (MCL 4125, MCL 4126, MCL 4187, MCL 4304, MCL 4304, MCL 4305 and MCL 4308). The proximal articular surface (Fig. 8F), concave and circular in outline, is contiguous medially with a crescentic facet for the ulna. Distal to the neck, the diaphysis widens mediolaterally (Fig. 8H–J). The length of the radius is nearly three times its maximum transverse width, which occurs distally (Fig. 8G).

Ulna. MCL 4201, MCL 4303 (Fig. 9A–D) and MCL 21273 are available for study. The former is the most robust. In anterior view the olecranon is inclined

medially (Fig. 9A). Below it and laterally (Fig. 9C, D), the surface for the humerus is expanded anteroposteriorly, and contiguous with the lateroposteriorly located and oval radial notch. The anterior and posterior margins of the diaphysis are straight and converge distally (Fig. 9C, D). The styloid process occupies the posterior part of the distal surface. The distal surface is oriented obliquely and expanded transversely (Fig. 9B), and bears a circular and flattened facet for the cuneiform.

Manus. Several elements of the manus of different individuals are preserved (see Supplemental Appendix 1). The manus of MCL 4303 is the most complete (Fig. 9E). Typical of Mylodontinae, five digits are present, the first three of which include osseous cores that in life bore claws. Those of digits two and three, similar in length and robustness, bear ungual phalanges with elongated and curved osseous cores. The ungual from digit one is shorter. Digits four and five are rudimentary. Mc V, similar in length to Mc III, has an oblique proximal surface, oriented distomedially, which bears the rounded and concave articular facet for the unciform and the triangular and flattened facet for Mc IV. Among the metacarpals, Mc IV is the longest and least rugose. Its proximal surface is distomedially oblique, and bears the articular facet for the unciform, which is contiguous medially with the two facets for articulation with Mc III. These two facets are located dorsally and ventrally and are separated from each other by a rough, nonarticular surface. Mc III is the most robust metacarpal; its length exceeds its greatest width, which occurs

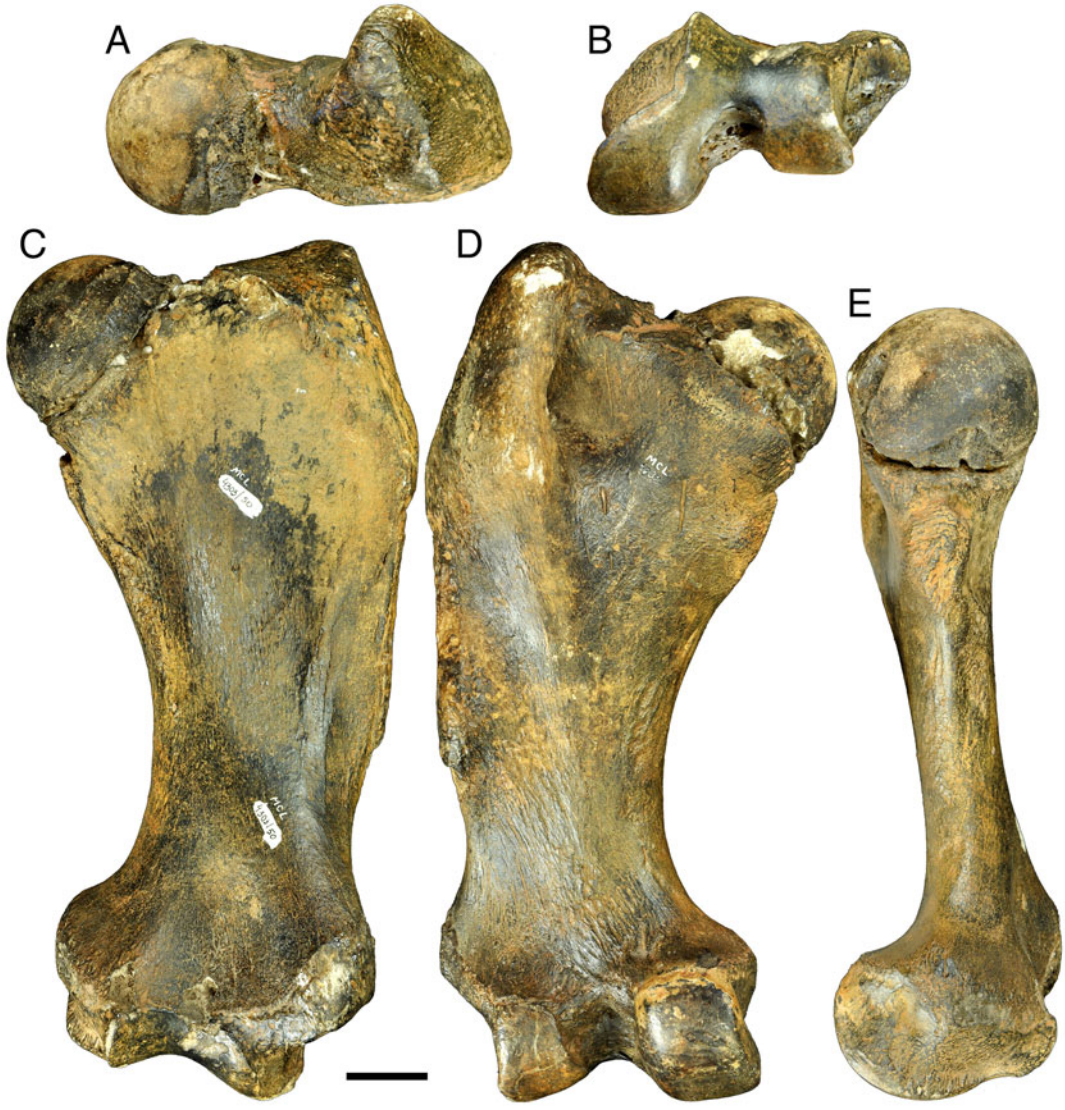

Figure 10. Left femur of *Glossotherium phoenesis* sp. nov. (holotype, MCL 4303) in proximal (**A**), distal (**B**), anterior (**C**), posterior (**D**) and medial (**E**) views. Scale bar = 50 mm.

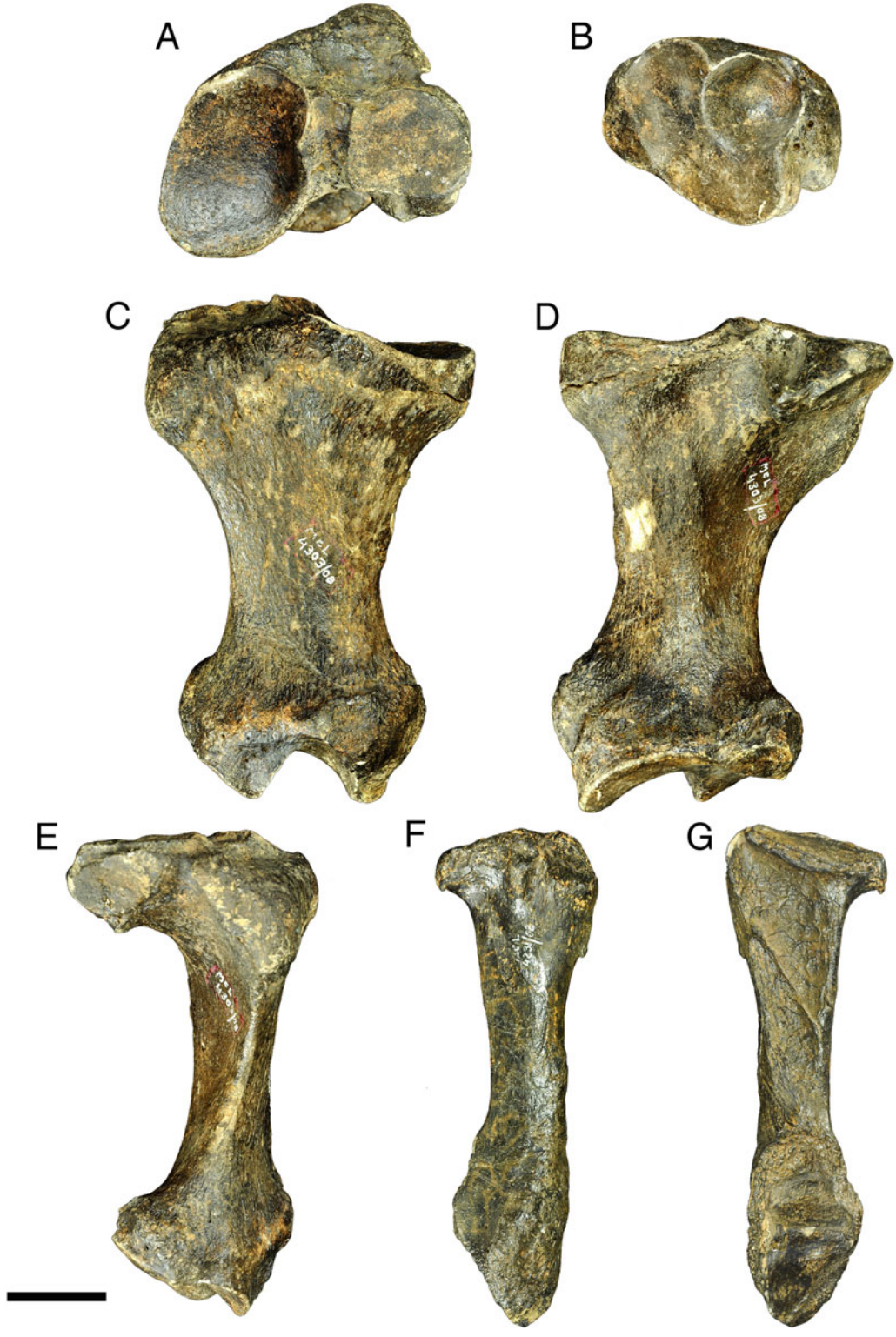

Figure 11. Tibia and fibula of *Glossotherium phoenesis* sp. nov. (**A–E,** holotype, MCL 4303; **F, G,** MCL 4231). **A–E,** right tibia in proximal, distal, anterior, posterior and lateral views, respectively; **F, G,** right fibula in anterolateral and medial views, respectively. Scale bar = 50 mm.

proximally (Fig. 9E). It is approximately 'T'-shaped, as its proximal surface expands medially and laterally. The medial expansion is less robust and projects less markedly than the lateral. It bears a convex facet for articulation with Mc II. On the proximal part of the lateral expansion lies a single facet for the magnum, whereas on the lateral surface there are two facets, separated by a rugose region, for articulation with the unciform. These two facets are contiguous with two facets, also separated from each other, on the distal part of the lateral expansion that articulated with Mc IV. Mc II, which is not preserved, must have had a proximolateral expansion that extended between the trapezoid and Mc III. Mc I and the trapezium are fused together. In dorsal view, the magnum is longer than wide (Fig. 9E). The maximal transverse width of the unciform is clearly exceeded by its proximodistal length. The trapezoid articulates with the scaphoid, magnum and Mc II. The pisiform is palmarly convex. The articular facet of the cuneiform for the pisiform is rounded, convex, and contiguous with the circular and flattened facet that articulates with the ulna.

Pelvic girdle. Of the pelvic girdle, only the right ischium and pubis of MCL 4303 are preserved (Fig. 7C, D), including part of the acetabular notch and the ventral portions of the lunate surface (major and minor, corresponding to the pubis and ischium). The obturator foramen is oval, and its midpoint height is approximately three times its width. The symphyseal region and the posterior margin of the ischium are not preserved.

Femur. Four specimens are preserved (see Supplemental Appendix 1), of which two are particularly well preserved. MCL 4231 belonged to an adult and MCL 4303 to a young adult (Fig. 10). In the latter, the process of ossification of the radius, tibia and, for the most part, the humerus had already been completed, but not of the head of the femur (Fig. 10C–E). In anterior view the medial margin is concave and the lateral margin is nearly rectilinear (Fig. 10A). The greatest constriction of the diaphysis occurs distally. Two patterns are observable: in MCL 4231 and MCL 4242 the head projects further proximally than the greater trochanter, whereas the reverse occurs in MCL 4303 (Fig. 10C, D). These different patterns are likely explained by sexual dimorphism, as the first two specimens are larger. Distally, the medial articular condyle is thicker than the lateral articular condyle. The proximal and middle third of the lateral margin are nearly rectilinear, but the distal third is concave (Fig. 10C, D).

Tibia. Among the specimens preserving the femur, MCL 4303 (Fig. 11A–E) and MCL 4231 also preserve the tibia and calcaneum. The latter specimen also preserves the fibula (Fig. 11F, G) and astragalus (Fig. 12A–C). The tibiae of these specimens are nearly identical morphologically, with MCL 4231 being larger. Proximally, the articular surface for the lateral femoral condyle is flattened and circular and is separated by a rugose sulcus from the facet for the medial femoral condyle (Fig. 11A). The latter facet is concave, ovate, with an oblique major axis and larger in area than the facet for the lateral femoral condyle. The facet for the lateral femoral condyle extends onto a proximolateral projection, which bears on its distal surface a flat and oval facet for articulation with the fibula. The medial margin of the diaphysis is wide and convex, whereas the lateral margin is narrower, forming a ridge (Fig. 11C–E). The posteromedial sulcus for the passage of tendons lies distally (Fig. 11B, D). Three articular surfaces are present distally (Fig. 11B). That for the fibula lies laterally and is flat, semicircular and contiguous with that for the proximolateral portion (i.e. discoid facet) of the astragalus. The surface is 'C'-shaped and concave, tangential to the articular surface for the fibula and occupies the anterior and posterior portions of the distal tibial surface (Fig. 11B). The surface destined for the odontoid process of the astragalus lies anteromedially. It is concave and contiguous with that for the discoid facet.

Fibula. The fibula (MCL 4231 and MCL 4115) is more robust distally than proximally, although its proximal end is expanded anteroposteriorly. The lateral surface of the diaphysis is transversely convex and smooth (Fig. 11F, G). Its medial surface is rugose and transversely concave. The proximal articular surface for the tibia is oblique, flattened and oval, with its major axis oriented anteroposteriorly. The distal epiphysis bears medially two contiguous articular surfaces. The more distal, articulating with the astragalus, is nearly triangular, flattened and faces distomedially. The other facet, for the tibia, is semicircular, flattened and faces proximomedially, meeting the tibial facet nearly at right angles.

Pes. Of the pes, only the astragalus (MCL 4231, Fig. 12A–C; also MCL 4115, MCL4307, MCL 4310 and MCL 4328), calcaneum (MCL 4303, Fig. 12D–F, MCL 4304, MCL 4304 and MCL 4306), cuboid (MCL 4115, Fig. 13A, B), navicular (MCL 4115, Fig. 13C–E), ectocuneiform (MCL 4115, Fig. 13F–H), Mt III (MCL 4377, Fig. 13I) and Mt IV and Mt V (MCL 4307, Fig. 13J; also Mt IV, MCL 21347 and MCL 4315; Mt V, MCL 4313) were recovered (see Supplemental Appendix 1). The calcaneum is typical of the genus. Its base is wide and rugose, with sides converging dorsally where they form a convex crest that descends

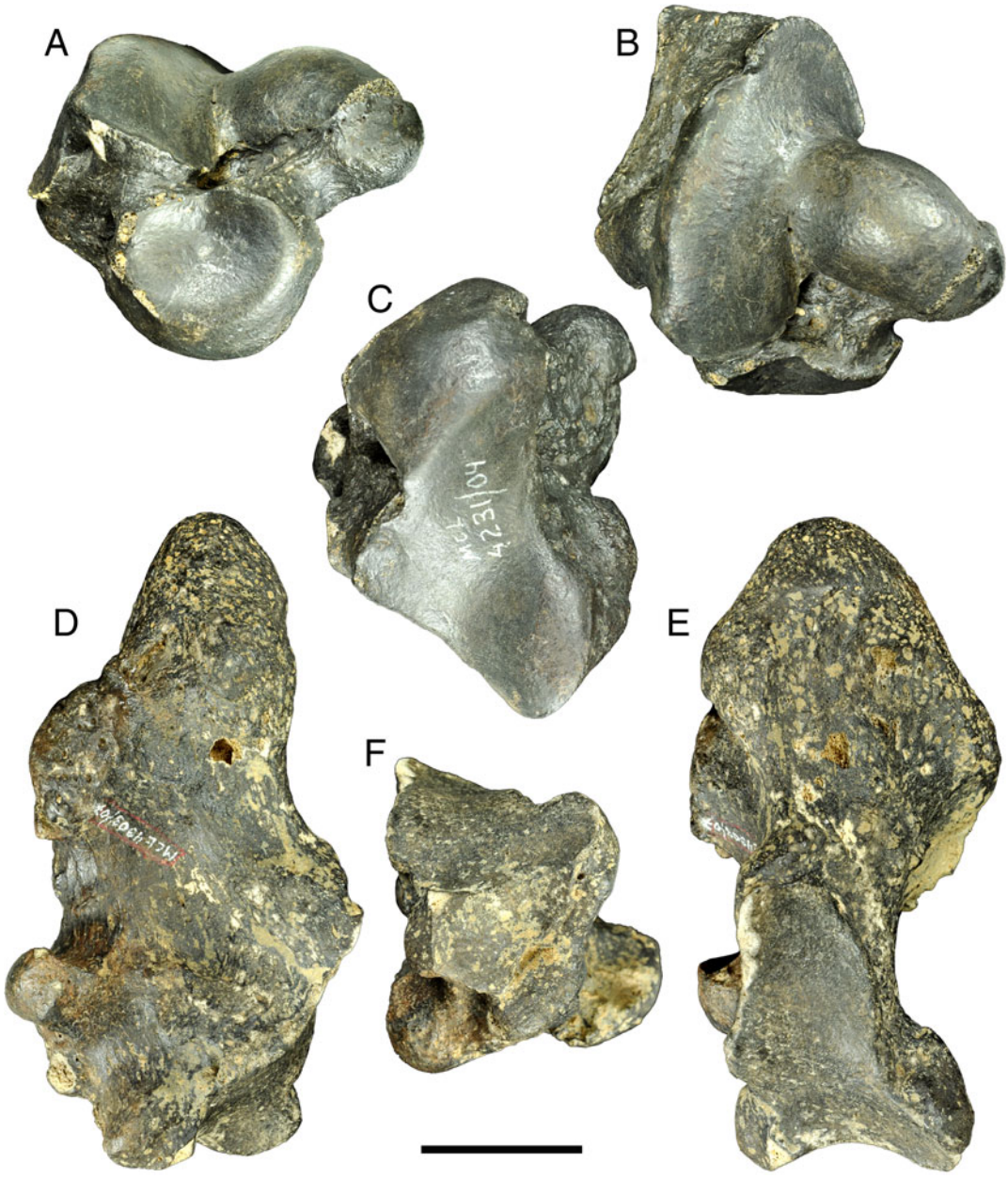

Figure 12. Astragalus and calcaneum of *Glossotherium phoenesis* sp. nov. **A–C,** right astragalus (MCL 4231) in anterior, dorsal and plantar views, respectively; **D–F,** right calcaneum (holotype, MCL 4303) in lateral, dorsal and proximal views, respectively. Scale bar = 50 mm.

posteriorly from the articular margin to the rugose tuber calcis (Fig. 12D–F). The anterior surface bears a basal rugosity (Fig. 12F). The mediolaterally concave cuboidal articular facet occupies less than half of the distal surface. Contiguous with this facet, on the proximodorsal surface of the cuboid, is the approximately triangular astragalar facet. Its surface undulates longitudinally and is oblique, rising dorsally. The facet occupies nearly half the length of the proximodorsal surface and narrows distally. The tuber calcis is transversely triangular with rounded lateral, medial and dorsal vertices (Fig. 12E).

Nearly the entire dorsal surface of the astragalus is occupied by the articular surface for the tibia (Fig. 12B). The tibial articular facet has two parts: a larger 'C'-shaped discoid facet on the anterior, lateral and posterior surfaces; and a facet that occupies nearly all of the anteromedially projecting odontoid process, the exception being its small anteromedial rugose portion. The articular surface for the fibula, contiguous

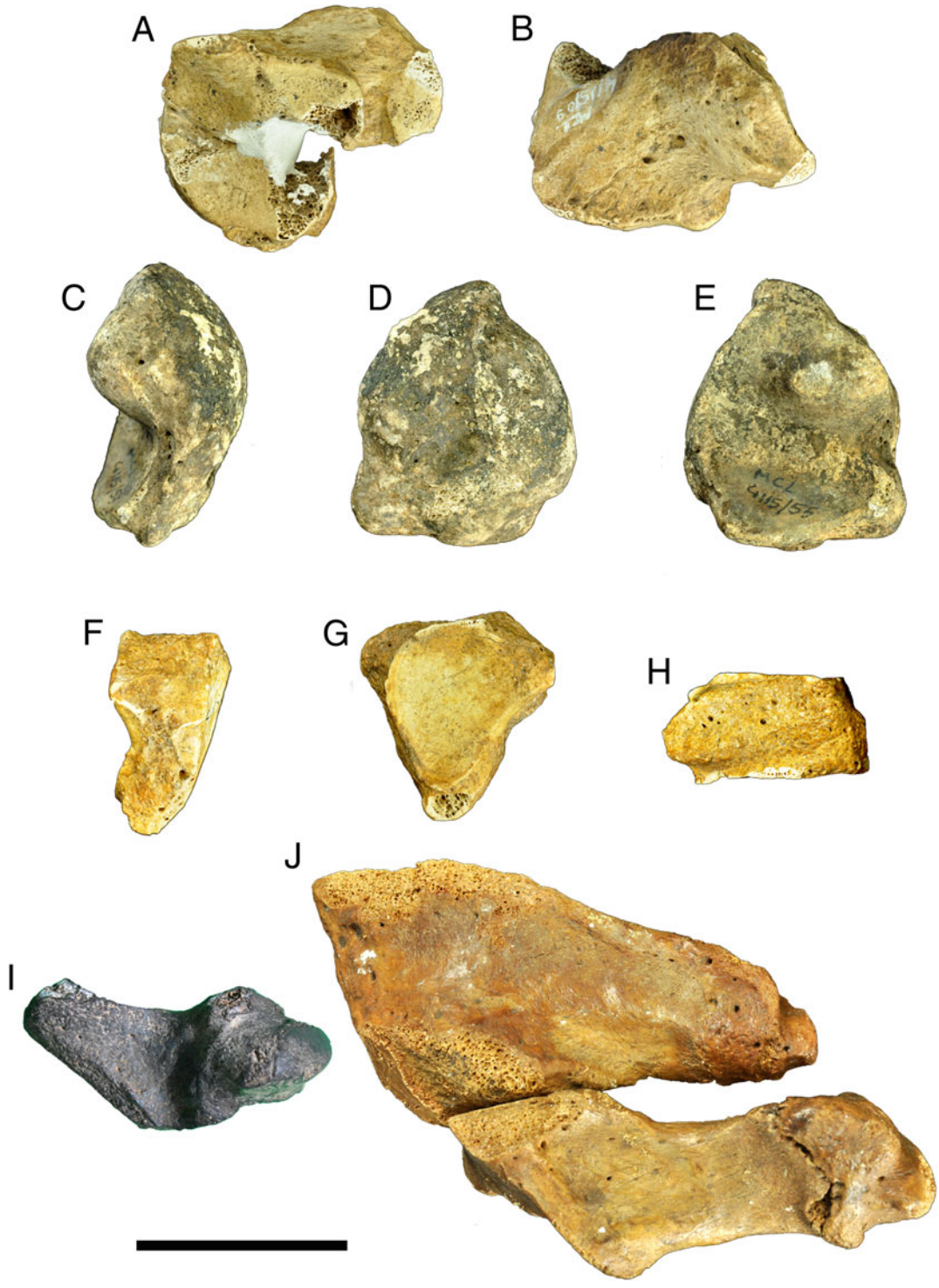

Figure 13. Tarsals and metatarsals of *Glossotherium phoenesis* sp. nov. **A, B,** left cuboid (MCL 4115) in proximal and dorsal views respectively; **C–E,** left navicular (MCL 4115) in medial, distal and proximal views, respectively; **F–H,** right ectocuneiform (MCL 4115) in lateral, proximal and dorsal views, respectively; **I,** left Mt III (MCL 4377) in dorsal view; **J**, left Mt IV-V (MCL 4307) in dorsal view. Scale bar = 50 mm.

with that for the tibia, is triangular and occupies a part of the lateral astragalar surface without reaching the calcaneal articular facet, which occupies the entire distal surface of the astragalus. The latter facet is contiguous with the cuboidal articular facet, which is distoplantar and convex. The cuboidal facet is also contiguous with

the navicular facet, which consists of a concave proximal part and a distal convex part (Fig. 12A). The medial surface of the astragalus lacks articular surfaces.

In the only cuboid available (MCL 4115), the proximal surface preserves nearly completely the concave astragalar articular surface (Fig. 13A, B). Contiguous laterally with the latter is the convex calcaneal articular surface, incompletely preserved. Medially it bears articular surfaces, also incompletely preserved, for the navicular and ectocuneiform. The distal surface preserves the dorsal part of the facets articulating with Mt V and Mt IV. Contiguous with the latter, dorsomedially on the distal surface, is the articular facet for Mt III. It is separated from the facet for the ectocuneiform by a non-articular and rugose sulcus.

The only navicular preserved (MCL 4115) is complete, triangular in distal view, and narrowing plantarly (Fig. 13C–E). The proximal articular facet for the astragalus is concave, and the distal articular facet for the Mt III is convex.

As noted by Owen (1842), only two cuneiform elements are present in *Glossotherium*. We follow this author's terminology for them as the entocuneiform and the ectocuneiform. The ectocuneiform is triangular, narrowing plantarly (Fig. 13F–H). The articular surface for Mt III is convex, which contrasts with the concave facet for the navicular. On the lateral surface, where it meets the dorsal surface, lie two facets, separated by a rugose region of bone, for articulation with the cuboid (Fig. 13F). The more distal of these facets is contiguous with the facet articulating with Mt III, and the proximal facet is contiguous with the navicular facet. There was no contact with the entocuneiform.

A prominent proximolateral extension of Mt III is a characteristic of Mylodontinae (MCL 4377; Fig. 13I).

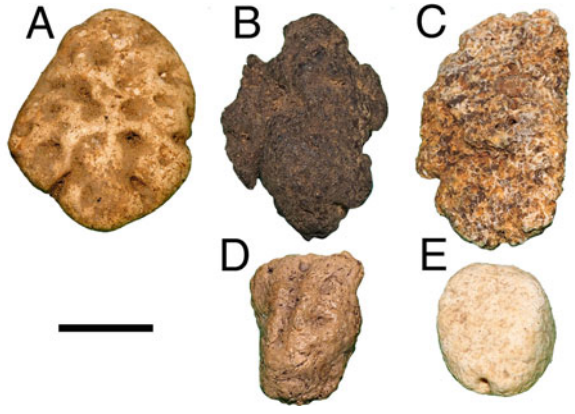

Figure 14. Isolated osteoderms in external view, from various species of Mylodontidae. **A,** *Glossotherium phoenesis* sp. nov. (MCL 21635). **B,** *Ocnotherium giganteum* (MCL 21640). **C,** *Valgipes bucklandi* (MCL 31631). **D,** *Paramylodon harlani* (MCL 21641). **E,** *Mylodonopsis ibseni* (MCL 21626). Scale bar = 10 mm.

On its proximal surface lies the articular facet for the ectocuneiform. Opposite this, on its distal surface, is the keeled articular surface for Mt IV. On its lateral surface, between the facets just noted, lies the articular surface for the cuboid. The greatest thickness of Mt IV occurs proximally, due to the presence of a plantar projection (Fig. 13J). A triangular articular surface, located proximolaterally, served for articulation with Mt V. Medially contiguous with this facet is the flattened, oblique articular surface that forms an acute angle with the lateral surface of the bone. This articular area, which occupies the proximal third of this skeletal element, served for articulation with the cuboid and is contiguous with the facet for Mt III, which is concave and approximately circular. The distal surface of Mt IV is occupied by an articular facet that bears a median keel and articulated with the proximal phalanx of digit IV. In dorsal and plantar views, Mt V resembles a right-angled triangle, with distal apex and proximal minor side (Fig. 13J). It is curved plantarly as the element's distal and proximal plantar surfaces are thickened. On its shorter, proximomedial side lies the cuboidal articular facet, which is rectangular, concave and oriented dorsoventrally. Medially this facet is contiguous with the triangular and plantarly narrowed articular facet for Mt IV. Distally lies a convex facet articulating with a rudimentary phalanx. The lateral surface of Mt V, its longest side, is narrow in the middle and expanded at its extremities.

Osteoderms

Osteoderms are known from three individuals: MCL 4303, the holotype, as well as MCL 4307 and MCL 4115 (see Supplemental Appendix 1). For reasons of institutional organization, these received different catalogue numbers than those assigned to the rest of the individuals: MCL 21635 (Fig. 14A), MCL 21364 and MCL 21620, respectively. However, there is no doubt that the osteoderms are associated with the remains of these individuals, as they were discovered lying undisturbed on several of their skeletal elements. Their size ranges from 5 mm to 30 mm. Some 2500 osteoderms are known from MCL 21620 (which corresponds to the specimen MCL 4115). Those representing the middle of the size range are the most abundant, and tend to be oval, compressed and biconvex. One surface usually bears numerous vascular foramina, whereas few, if any, are observable on the opposite side.

Comparisons and remarks

Comparisons of several characters of the new species to other mylodontines, particularly the two South

American Pleistocene *Glossotherium* species, *G. robustum* and *G. tropicorum* (see Material and methods), demonstrate its specific distinctness. Intraspecific differences are also noted, particularly as these relate to the two well-preserved skulls of *G. phoenesis*, as these differences may be attributable to sexual dimorphism.

On the anterior margin of the maxilla the notch medial to the Cf1 is less prominent in *G. tropicorum* than in *G. phoenesis* (Figs 2B, 3B) and is not present in *G. robustum*. Also, the middle part of the maxillary margin projects more strongly in *G. tropicorum* than in *G. phoenesis*. The maximal length of the palate is twice the width between the caniniforms in the new species (Figs 2B, 3B; Supplemental Appendix 2), whereas in *G. tropicorum* and *G. robustum* the length exceeds the width only slightly. The ventral margin of the foramen magnum is arch-shaped in *G. phoenesis* and *G. robustum*, but markedly acute in *G. tropicorum*. In the latter, the margin of the pterygoid in ventral view is curved, being concave laterally, whereas it tends to be more nearly rectilinear in *G. phoenesis.*

G. tropicorum and *G. robustum* differ with respect to *G. phoenesis* in the implantation of the upper teeth: in the first two species a line through the tooth row intersects the vestibulolingual midpoints of the occlusal surface of each tooth; and the lines from the left and right side tooth rows converge posteriorly and meet at an angle of approximately 22° in *G. tropicorum* and, based on images in Owen (1842) and Lydekker (1894), 25° in *G. robustum*. In *G. phoenesis*, as noted above, such a line intersects the midpoint of only the last three teeth, with Cf1 and Mf1 displaced laterally, and left and right molariform tooth rows are nearly parallel to each other (Fig. 5B, C). In *G. phoenesis* (Figs 2B, 3B; Supplemental Appendix 2) and *G. robustum* the maximal width across the parietals is clearly less than that across the paroccipital processes, but these widths are nearly equal in *G. tropicorum.*

Differences in proportions of the skull among *Glossotherium* species are revealed in the length of the palate (excluding the premaxillae) in relation to the width between the Mf4s (Supplemental Appendix 2). In *G. phoenesis* the length is nearly twice the width in MCL 4303 (Fig. 2B) and MCL 4027 (Fig. 3B). This ratio is less, approximately 1.5, in *G. tropicorum* and *G. robustum*. A difference in proportion also occurs in the length between the anterior margin of the zygomatic process of the squamosal and the zygomatic process of the frontal, compared with the width across each set of these processes. The length exceeds the widths in *G. phoenesis*, whereas the reverse is true in *G. robustum* and *G. tropicorum*.

The greatest height of the skull of *G. phoenesis* occurs between the ventral margins of the pterygoids and the dorsal convexity of the frontals at the level of the optic foramen. In *G. tropicorum* this occurs more posteriorly, at the level of the foramen ovale. In the latter, the posterior margin of the skull, corresponding to the supraoccipital, is more oblique compared to the skull's dorsal margin. The two species differ as well in the degree of projection of the pterygoids. In *G. tropicorum* they are expanded ventrally. Ventral to the zygomatic arch the height of the pterygoid is twice that of the zygomatic arch, but in *G. phoenesis* the two heights are nearly equal (Figs 2C, 3A). The outline of the posterior, or occipital, surface tends to be sub-oval, wider than high, in *G. robustum*. In *G. tropicorum* it is subcircular, whereas in *G. phoenesis* (Figs 2C, 3A), as in *G. robustum*, it is wider than high, but outlines a wide arch.

In the ear region, some differences can be detected among the three species of *Glossotherium*. The entotympanic of *G. phoenesis* is elongated in MCL 4303 (Figs 2B, 4) whereas it has a blocky shape in MCL 4027 (Fig. 3B). The same characteristics were recognized for *G. robustum* by Boscaini *et al.* (2018), who stressed the intraspecific variation of this feature. For *G. tropicorum* only the blocky conformation of the entotympanic is currently known (De Iuliis *et al.* 2017). The occipital artery is partially closed into a bony canal in *G. phoenesis* and *G. tropicorum*, whereas in *G. robustum* this artery is almost completely enclosed in it. Consequently, the ventral opening of the occipital artery is positioned more posteriorly in *G. phoenesis* and *G. tropicorum* than in *G. robustum*.

In lateral view, the mandibular condyle of *G. phoenesis* (Fig. 2F) is clearly more ventral than in *G. robustum* and *G. tropicorum* relative to the plane that is tangential to the occlusal surface of Mf4 and the dorsal symphyseal margin. Consequently, in the latter species the space between the posterior margin of the coronoid process and the mandibular condyle is smaller. The morphology of the angular process differs considerably: short, high and with a relatively narrow notch ventral to the condyle in *G. tropicorum* and especially *G. robustum*, whereas it is elongated and with a wider notch in *G. phoenesis* (Fig. 2F, G). In the latter, the condyle projects more medially than laterally (Fig. 2H), whereas the reverse occurs in *G. tropicorum*.

A notable difference between *G. robustum* and the two intertropical species occurs at the mandibular symphysis. Its width exceeds tooth row length in *G. robustum*, whereas the reverse is true in *G. tropicorum* and *G. phoenesis* (Figs 2H, 5D). However, these last two species differ in the position of the lower teeth. A line

extending through the occlusal midpoints of the molariform teeth passes tangentially to the lingual surface of cf1 and the lateral surface of the symphyseal spout in *G. phoenesis* (Figs 2H, 5D), whereas in *G. tropicorum* it passes through the midpoint of cf1 and lateral to the margin of the spout. In *G. robustum* it passes medial to both the cf1 and the margin of the spout. These differences reflect the lateral expansion of the spout in the latter species compared to the narrower spout in the intertropical species.

The differences among the species of *Glossotherium* with regard to the morphology of the dentition have already been emphasized. Among the less notable differences is the more marked apicobasal sulcus on the lingual surfaces of Mf2-Mf3 of *G. phoenesis* (Fig. 5B, C). A main difference between the teeth of *G. phoenesis* and *G. robustum* occurs in Cf1 and Mf1. In the latter species they tend to be of circular section. In *G. phoenesis* cf1 tends to be larger, and oval or triangular, and Mf1 is oval (Fig. 5B, C), as also occurs in *G. tropicorum*. A notable difference between the latter and *G. phoenesis* occurs with Mf1, which did not wear against cf1 but only with mf1 in *G. tropicorum*. Thus, the wear between the distal surface of cf1 and the mesial surface of Mf1 evident in these teeth of *G. phoenesis* did not occur in *G. tropicorum* (see De Iuliis *et al.* 2017). The distal portion of Mf2 and mf1 is narrow and elongated in *G. phoenesis* (Fig. 5A, E), whereas these portions in *G. tropicorum* and *G. robustum* are shorter.

The seven dentaries available for *G. phoenesis* encompass several life stages, from very young (MCL 4014, MCL 4015) individuals to older adult (MCL 4008) individuals. This sample reveals that individuals of this species were born with erupted dentition, which has also been noted for other Folivora based on specimens in MCL (see also Naples 1990). Cartelle *et al.* (1989) described the mandibular body of the scelidotheriine *C. cuvieri*, noting that the dentition erupted in unison. The described specimen (MCL 4248) was of an extremely young and probably newborn individual. A specimen of the nothrotheriid *N. maquinense*, MCL 2825, was preserved and recovered from the pelvic region of its presumed mother and thus was considered as still in utero. Its teeth were erupted and exhibited apical wear (Cartelle 2012). Recently Cartelle *et al.* (2014) illustrated the teeth of very young individuals of the giant megatheriine *E. laurillardi*, among them MCL 31616, a portion of dentary preserving four molariforms of, probably, a newborn individual. As in the dentary of *N. maquinense*, the teeth were conical and exhibited apical wear. These examples strongly suggest that in extinct sloths the eruption of teeth by birth may have been the normal condition. This also occurs in modern sloths (see Naples 1982).

It is clear from specimens of both juvenile and adult individuals of *G. phoenesis* that the depth of the dentary at mf3 is greater than that at cf1 (Fig. 2F, G; Supplemental Appendix 2) and that the maximal width of the symphyseal spout is less than the distance between the left and right cf1s (Fig. 2H). These proportions, as well as the relative width (i.e. thickness) of the dentary compared to molariform width, were thus maintained throughout growth. In contrast, Cartelle *et al.* (2014) noted that in the ontogenetic development of the dentary of *E. laurillardi* the width of the dentary with respect to the molariforms decreased as the animal grew from a juvenile to an adult (i.e. with age the molariforms became relatively wider), and that the depth of the dentary increased, particularly at the level of the more distal molariforms. The differences expressed during ontogenetic development between these species are possibly related to the development of the dentition. In *E. laurillardi* (Cartelle & De Iuliis 2006) the molariforms of very young individuals are larger basally than apically, so that they are conical (tapering apically). In older juveniles the mesial and distal surfaces become parallel to each other, whereas in adults the molariforms are larger apically than basally (Cartelle 1994). This last phase does not occur in the new species being described: the mesial and distal surfaces are parallel in juveniles and adults.

Several morphological differences noted in the descriptions of *G. phoenesis* are related to age, including those of the dentition. Among them are accentuation of the trilobate form of mf1 and increased depth of the sulci of mf2 (Fig. 2H). The most notable changes occur in mf3. On the mesial lobe the mesial margin transformed from convex to concave and the vestibular portion became longer and narrower than the lingual; on the distal lobe, the lingual portion became more accentuated than the vestibular; and the isthmus, connecting the lobes, was short in very young individuals but elongated to nearly the same length as the mesial lobe in adult individuals.

De Iuliis *et al*. (2017) noted that in the axis of *G. tropicorum* the articular facet of the odontoid process is contiguous on either side with the atlantal facets. This morphology does not occur in the available three specimens of *G. phoenesis* in the MCL collection (Fig. 6D–G). These facets are also separate in other Brazilian sloths, such as the mylodontid *O. giganteum*, the scelidotheriines *V. bucklandi* and *C. cuvieri*, and the nothrotheriid *N. maquinense*. Contiguous facets are by far the more common condition in the megatheriid *E. laurillardi*, in which 32 of 34 specimens housed in MCL bear

contiguous facets, suggesting that this was the usual pattern in this species.

The articular surface of the odontoid process is oriented more obliquely in *G. phoenesis* than in *G. tropicorum* and *G. robustum*. In the axis of the latter species the spinous process is the portion projecting furthest, whereas in *G. phoenesis* this region is short and its most posteriorly projecting part (on either side) is the margin of the posterior zygapophyses (Fig. 6G).

According to Hoffstetter (1959), the asymmetry between the right and left pedicles of the neural arch of some thoracic vertebrae (see above and Fig. 6J) results from accommodating the emergence from the vertebral canal of a branch of the intrarachidian vein, and is observed in the collections of MCL specimens of Nothrotheriidae (MCL 1020), Megalonychidae (MCL 22875), Mylodontidae (MCL 4304) and Megatheriidae (MCL 33075). Although Engelmann (1985) considered this a synapomorphy of all Folivora or Tardigrada, not all specimens display this morphology, with several possessing symmetric right and left pedicles.

Comparison between the humerus of *G. phoenesis* (Fig. 8A–E) and *G. tropicorum* reveals several differences. The deltopectoral crest is more prominent and rugose in the former (Fig. 8C), and its medial diaphyseal margin is strongly curved and passes mediodistally, just past the level of the deltopectoral crest, into the large and proximally projecting entepicondyle. In these regards it resembles the condition in *G. robustum*. In *G. phoenesis*, however, the medial margin is less markedly curved and extends further distally beyond the shelf before curving toward entepicondyle. Compared to the humerus of *G. robustum* that of *G. phoenesis* bears a more proximally projecting greater tubercle and more distally expanded ectepicondyle and entepicondyle. Also, the lateral margin of the deltopectoral crest is more obliquely oriented and projects more strongly laterally. Overall, the humerus of the Brazilian species is more gracile (Fig. 8C–E). The radius of *G. robustum* and *G. tropicorum* are similar in shape and proportions, with the maximum width occurring near the distal end. The olecranon process of the ulna is shorter and the articular surfaces for the radius and humerus are, respectively, longer and narrower in *G. robustum* than in *G. phoenesis* (Fig. 9A–D).

The manus of *G. robustum* and *G. phoenesis* are morphologically similar. Among the differences are that in *G. phoenesis* the dorsal surface of the magnum is longer than wide, whereas the reverse is true in *G. robustum.* The proximomedial portion of Mc III, for articulation with Mc II, is smaller than its proximolateral portion, for articulation with Mc IV (Fig. 9E), whereas the reverse occurs in *G. robustum*. Owen (1842) reported that in *G. robustum* the size of the ungual phalanges increases progressively from the first to third digits, but in *G. phoenesis* the ungual phalanges of digits two and three are nearly equal in size (Fig. 9E). In the manus of the mylodontid species *V. bucklandi* (MCL 4293), *C. cuvieri* (MCL 4265) and *O. giganteum* (MCL 4229), the phalanges of digit three are larger than those of digit two, whereas in *Mylodonopsis ibseni* (MCL 450) the phalanges of these digits are nearly equal in size, as in *G. phoenesis.* For the manus of *G. tropicorum* only the unciform, cuneiform and Mc IV are known (see De Iuliis *et al.* 2017). The unciform of this species possesses two articular facets for the magnum and two for Mc III, but in that of *G. phoenesis* there are two distal facets, one dorsal and the other palmar, for Mc III but only a single facet for the magnum, with an isthmus uniting the dorsal and ventral portions. Among the differences between the cuneiform of *G. tropicorum* and *G. phoenesis* are that the lateral border is nearly straight in the former but concave in the latter, and the articular facets for the ulna and pisiform are contiguous in *G. phoenesis* and separate in *G. tropicorum*. In the cuneiform of *G. robustum* "the sides of its base are so produced as almost to equal the length of the bone" (Owen 1842, p. 92), but in *G. phoenesis* (MCL 4304) the length of the cuneiform is clearly greater than its proximal width. Mc IV of *G. phoenesis* is gracile and has a markedly oblique proximal articular margin, whereas that of *G. tropicorum* is more robust and has a less oblique margin. The proximal articular surfaces differ in that the facet for the magnum in *G. tropicorum* is arched as compared to nearly right-angled in *G. phoenesis*. In MCL 4303 the proximolateral facet for Mc III is contiguous with that for the magnum, but these are separate in *G. tropicorum* (ROM 5515).

Glossotherium robustum and *G. phoenesis* are very similar in femoral and tibial morphology. Esteban (1996) considered the separation of the facets for the tibia and astragalus distally on the fibula (also recognized by Owen 1842) as a diagnostic character of *G. robustum*. In *G. phoenesis* these facets are contiguous.

The calcaneum of *G. phoenesis* and *G. robustum* are also very similar morphologically. The odontoid process of the astragalus of *G. phoenesis* is narrower and more obliquely oriented anteriorly and the facet for articulation with the calcaneum projects less distally (Fig. 12B), which results in a more prominent posterior or distal margin in *G. robustum*. The femur, fibula, astragalus and calcaneum are not known for *G. tropicorum*. The ectocuneiform of *G. phoenesis* does not contact the entocuneiform. In addition to the articular surfaces for the navicular and Mt III, the ectocuneiform bears a proximal and a distal facet on its lateral surface for the cuboid. There is thus a difference and a

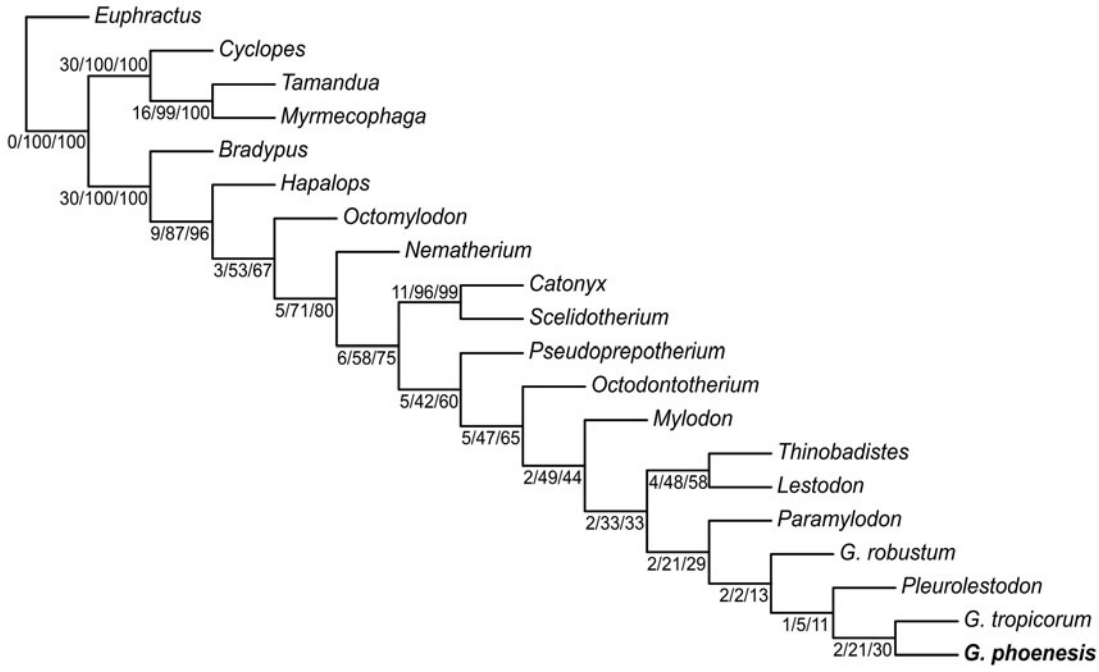

Figure 15. Most parsimonious tree (MPT; length = 764 steps, CI = 0.656, RI = 0.927) obtained based on phylogenetic analysis using TNT (Goloboff *et al.* 2008a, b) reporting support values (respectively from left to right Bremer support, bootstrap and jackknife values).

similarity with the homologous element of *G. robustum*; according to Owen's (1842, p. 120) description it "presents only two articular surface, a posterior one, slightly concave, for the navicular, and an anterior one, in a less degree convex, for the oblique base of the middle metatarsal" and "there is no trace of an articular surface for the cuboides on the outer margin, or for a middle cuneiform bone on the inner one". Mt IV of *G. phoenesis* (Fig. 13J) is less robust than that of *G. robustum* and *G. tropicorum*. The articular surfaces for the cuboid and Mt III are more oblique, compared to the long axis of the element. In *G. tropicorum* the articular surface for the cuboid is narrow, with a curved lateromedial margin. It is isolated from and larger than the facet for Mt III. By contrast, in *G. phoenesis* the cuboidal facet is circular, nearly equal in size to and contiguous with that for Mt III. The Mt V of *G. robustum* and *G. phoenesis* (Fig. 13J) is generally triangular. That of *G. robustum* has a nearly rectilinear lateral margin, whereas this margin is concave in *G. phoenesis*, owing to expansion of the proximal and distal ends of the element, which also causes a concavity on its ventral or plantar surface.

Phylogenetic analysis

The character matrix is that of Gaudin (2004), compiled using Mesquite (Maddison & Maddison 2011), with modifications of two characters (char. 6 and 25) and in taxon selection (Supplemental Appendices 5 and 6). We kept the 286 osteological characters of the skull, lower jaw, dentition and hyoid arch used by Gaudin (2004). However, we modified the definition and states of characters 6 (ordered) and 25 (unordered) as follows: char. 6 diastema between Cf1 and Mf1: (0) absent, (1) moderate (<1/2 of the anteroposterior length of the Cf1) and (2) elongated (>1/2 of the anteroposterior length of the Cf1); and char. 25 diastema between Mf1 and Mf2: (0) absent and (1) moderate (<1/2 of the anteroposterior length of the Mf1). In the phylogenetic analysis performed by Gaudin (2004), the taxon *Glossotherium* grouped together several specimens of *G. robustum* and *G. tarijensis*. In our new analysis, we codified only *G. robustum* (pending a reconsideration of the species *G. tarijensis*), and coded *G. tropicorum* (De Iuliis *et al.* 2017) and the new species *Glossotherium phoenesis* (Supplemental Appendices 4 and 5) as separate species. Fourteen mylodontid species comprised the ingroup and, following Gaudin (2004), we maintained six outgroups (i.e. the armadillo *Euphractus*, the anteaters *Cyclopes*, *Tamandua* and *Myrmecophaga*, the primitive Megatherioidea *Hapalops* and the modern tree sloth *Bradypus*). The complete phylogenetic dataset (Supplemental Appendix 5) was analysed using the parsimony software TNT v. 1.0 (Goloboff *et al.* 2008a, b).

The phylogenetic analysis results in a single most parsimonious tree (tree length 764 steps, CI = 0.656, RI = 0.927; Fig. 15). *Glossotherium phoenesis* sp. nov. is the sister taxon of the tropical species *G. tropicorum*. This node is relatively well supported, with bootstrap and jackknife values of 21 and 30, respectively. The unambiguous synapomorphies which support this node are: moderate diastema between Cf1 and Mf1 (<1/2 of the anteroposterior length of the Cf1; modified from Gaudin 2004: char. 6^1); moderate diastema between Mf1 and Mf2 (<1/2 of the anteroposterior length of the Mf1; modified from Gaudin 2004: char. 25^1); and an intermediate development of the coronoid process (ratio of maximum height to anteroposterior length measured at mid height ≤1.25, >1.0; Gaudin 2004: char. 47^1). *Pleurolestodon* appears as the sister taxon of the clade formed by the two previous taxa (*G. phoenesis* + *G. tropicorum*), making the genus *Glossotherium* paraphyletic. The clade (*Glossotherium* + *Pleurolestodon*) is supported by three synapomorphies: Cf1 located right at the anterior edge of the maxilla (Gaudin 2004: char. 21°); braincase width ≥25%, <30% of basonasal length (BNL; Gaudin 2004: char. 82^2); and occipital condyles widely separated (with a minimum distance between them in ventral view >10% of BNL; Gaudin 2004: char. 186°).

Our results, suggesting the paraphyly of *Glossotherium*, have several implications. One is that *G. phoenesis* and *G. tropicorum* could be assigned to *Pleurolestodon*, rather than *Glossotherium* as understood from the classically known and much more abundantly represented *G. robustum*. Conversely, *Pleurolestodon* could be considered a synonym of *Glossotherium*, which would then include at least four species. Yet another possibility is that we accept the results of our analysis as conclusive and erect a new genus for the reception of *G. tropicorum* and *G. phoenesis*. However, there are several reasons from refraining, for the time being, from choosing decisively among these possibilities, rather than following the course that we have taken. Although *Pleurolestodon* is a valid genus, it was described by Rovereto (1914) on Huayquerian (late Miocene) remains and is about one-third to one-half the size of the three species, all Pleistocene in age, assigned here to *Glossotherium*. Also, precise understanding of aspects of its taxonomy remains problematic. For example, there appears to be only a single valid species (see Boscaini *et al.* 2019), and only one skull (FMNH 14495), as the original type (housed in MACN) is apparently lost. Certainly, these facts alone would not preclude a closer affinity of *Pleurolestodon* to *G. tropicorum* and *G. phoenesis*, but given that our analysis is also based only on craniodental evidence, we believe that making a drastic systematic decision would be premature; and that it would be more prudent to wait until more comprehensive data, including representation from the postcranial skeleton, are available for phylogenetic analysis. Extensive codification of such postcranial characters is not currently available in the literature on mylodontids, but this subject matter is a major component of the ongoing doctoral research of one of the authors (AB). Pending phylogenetic analysis based on such data, as well as the craniodental evidence, we therefore refrain from making a major taxonomic rearrangement. We expect that the relationships among these mylodontids will be clarified with AB's research, and preliminary results do suggest that the three *Glossotherium* species cluster together. We cannot, for obvious reasons, be more specific in this regard. Our assignment here of the new species to *Glossotherium* is based on the greater overall resemblance of this new species to already described *Glossotherium* species than to *Pleurolestodon*.

Possible dimorphism in the new species

Lydekker (1894, p. 79) was the first author to consider dimorphism in Mylodontidae in his assessment of '*Mylodon robustus*' (= *Glossotherium robustum*), in which he synonymized 14 species: "From a survey of some five-and-twenty more or less nearly complete skulls … I am convinced thut [sic] the whole of the long list of names given above are synonyms of this species; those names having been applied to specimens differing from one another by characters due either to sex, age, or individual variation". This author (Lydekker 1894, pl. 49) also figured skulls that he attributed to male and female individuals.

Although other authors (e.g. Cabrera 1936) did not reach the same conclusions as Lydekker, they nevertheless recognized distinctions based on robust (*G. robustum*) versus gracile (*G. lettsomi*) species. In contrast, Cartelle & Bohórquez (1982), Cartelle & De Iuliis (1995, 2006), as mentioned, as well as De Iuliis & Cartelle (1999), also noted the likelihood of sexual dimorphism in the megatheriids *E. laurillardi* and *Eremotherium eomigrans*, respectively. Dimorphism is manifest in the patterns of size differences that occur in the postcranial elements of young and adult individuals and in skull morphology. In the same vein, Prothero & Raymond (2008) attributed size variation as indicative of sexual dimorphism in terrestrial sloths. Also, McDonald (2006) attributed differences in skull morphology in *Paramylodon harlani* as sexual dimorphism (see below).

Employing measurements and figures, Esteban (1996) demonstrated appreciable intraspecific variation in *G. robustum* that, we suggest, might be related to sexual dimorphism (see Supplemental Appendix 2). Comparative measurements of *P. harlani* and *G. robustum* published by McAfee (2009) indicate clear intraspecific variation that might also be interpreted in this same way.

The criteria for sexual dimorphism recognized by McDonald (2006) in his analyses of *P. harlani* involved some skulls being more gracile than others, cranial constrictions, palatal width, inclination of the occipital region and, as a consequence, differences in projection of the occipital condyles, and in the form and wear of the caniniforms. These distinguishing features are present in the two main skulls (MCL 4003 and MCL 4027; Figs 2A–D, 3A–D) discussed in the current report. The differences regarding the caniniforms described for *P. harlani*, i.e. that the Cf1s are more robust and curved than the cf1s, are barely apparent in the new species, nor do the cf1s show reduced wear as described by McDonald (2006). However, there are clear differences between the Cf1s of the two *G. phoenesis* specimens that we interpret as indicating dimorphism: in MCL 4003 the Cf1 is semicircular in section and small in area (Fig. 5B), whereas in MCL 4027 the Cf1 is larger and triangular in section (Fig. 5C). In addition to the features identified by McDonald (2006), there are proportional and anatomical differences among the various specimens of *G. phoenesis* in the dentition, mandible and long bones. These provide convincing support for the interpretation of sexual dimorphism, a hypothesis reinforced by the fact that the differences are not so much discrete as proportional. It is important, in this regard, to reiterate that the specimens analysed here were recovered from the same locality and horizon, with the exception of an astragalus, MCL 4310, that was collected from a cave in Lagoa Santa (Minas Gerais). This specimen expands the known distribution of the new species (Cartelle 2012).

The variation recorded by Miño-Boilini & Zurita (2015) in their analysis of numerous skulls of Scelidotheriinae was interpreted as evidence of sexual dimorphism. The remains analysed here, including skulls MCL 4027 and MCL 4303, adult mandibles MCL 4003 and MCL 4008, and long bones, e.g. the femora MCL 4303, MCL 4231 and MCL 4242, exhibit similar variations that suggest that sexual dimorphism is also a likely explanation.

Such studies have provided the basis for the trend, over the last 20 or so years, for the invalidation of the numerous sloth species that were erected, as noted in the Introduction, based on small variations in size or morphology (e.g. Cartelle and De Iuliis 1995, 2006; De Iuliis *et al.* 2014; Boscaini *et al.* 2019). They indicate that the confident recognition of species, among Pilosa at least, requires a reasonable sample size. The differences recorded here, particularly as revealed by skulls MCL 4303 and MCL 4027, provide support for the recognition of sexual dimorphism, because the otherwise strong similarities in the dentition and general skull morphology of specimens from the same locality convincingly point to conspecificity. As noted above, MCL 4303, from a young adult individual, and MCL 4008, which was likely of similar age to MCL 4027, are among the mandibles available for analysis. Although MCL 4008 is larger than MCL 4303 and its caniniforms and molariforms are more robust, their tooth row lengths are similar.

Several differences between MCL 4027 and MCL 4303 (Figs 2A–D, 3A–D) are presented in Supplemental Appendices 2 and 3. The two specimens are of similar age, with MCL 4027 possibly being slightly older based on sutural closure. Other differences between these specimens are noted in the tables of measurements provided in this work (Supplemental Appendix 2). It is possible that the differences in the arrangement of the teeth in the two skulls and in various mandibles, including juveniles, may also reflect sexual dimorphism. The specimens with divergent tooth rows have large caniniforms (in juveniles as well), whereas specimens in which the molariforms are nearly parallel and only the caniniforms are positioned more laterally have smaller caniniforms. The degree of similarity between the two specimens in terms of skull sutures, dentition and general morphology, particularly of the basicranial region, strongly suggests they are conspecific. The evidence presented for dimorphism by McDonald (2006) for *P. harlani* and here for *G. phoenesis* lends support to a similar interpretation of differences in the skull of *G. robustum*, as was proposed by Lydekker (1894).

Osteoderms of intertropical Brazilian Mylodontidae

Osteoderms from Pliocene and Pleistocene mylodontids have been reported by several authors (e.g. Merriam 1906; Sinclair 1910; Stock 1925; Hoffstetter 1952; Hill 2006). The most well known are those of *Mylodon darwinii* recovered in association with skin in the Ultima Esperanza Cave in Chile (Moreno & Woodward 1899).

As noted above, osteoderms were recovered for several specimens of *G. phoenesis* (Fig. 14A). Other mylodontid species recovered from diverse localities are known to have possessed osteoderms, including *M. ibseni* (in which they are particularly abundant; e.g.

MCL 21626, Fig. 14E, MCL 21629 and MCL 21639), *O. giganteum* (e.g. MCL 21630 and MCL 21640, Fig. 14B) and *V. bucklandi* (e.g. MCL 21623, MCL 21642 and MCL 31631, Fig. 14C). Arzani *et al.* (2014) reported the presence of osteoderms in *G. robustum*; a second specimen of this species, deposited at the San Pedro Museo (Buenos Aires Province, Argentina), also preserves osteoderms (AB, pers. obs. 2017). Osteoderms have been recovered in *P. harlani* from Rancho La Brea (Stock 1925), including a few available for the present study (e.g. MCL 21641, Fig. 14D). The latter are more irregular than those of *G. phoenesis* (Fig. 14A).

In Brazil, Lund (1846) noted the presence of osteoderms in *N. maquinense* and '*Scelidotherium*' (i.e. *C. cuvieri* and *V. bucklandi*), and Cartelle & Bohórquez (1986) in *E. laurillardi*. However, this latter assignment is erroneous as are those, in part, proposed by Lund (1846). The osteoderms discussed by this latter author belong instead to *V. bucklandi*, as demonstrated by subsequently recovered material (Cartelle *et al.* 2009). The assignment of osteoderms to *E. laurillardi* by Cartelle & Bohórquez (1986) was shown to be incorrect by further work conducted by one of the current authors (C.C.) in the locality Toca da Onças ('Puma Cave', near Jacobina, Bahia, Brazil), from which the osteoderms were recovered. This researcher determined that the osteoderms instead belong to the mylodontid *O. giganteum*. McDonald's (2018) scepticism on the presence of osteoderms in *E. laurillardi* was, therefore, justified. It is also very probable that this author's suspicions on the presence of osteoderms in the closely related megatheriid *Megatherium americanum*, reported by Politis & Messineo (2008), will also be confirmed, given that there are no other reliable reports of osteoderms in Megatheriidae, including *M. americanum*, despite this clade's abundant fossil record. Lund's (1846) assignment of osteoderms to *N. maquinense* must also be considered suspect. Several nearly complete skeletons of this species, one of them in articulation and with coprolites, have been recovered by one of us (i.e. CC), but evidence of osteoderms was entirely lacking. Given the exquisite preservation and *in situ* recovery of several of the specimens, it is highly improbable that the lack of osteoderms is due to factors other than their absence in this species.

The remains of *G. tropicorum* recovered from Corralito (Ecuador) and Talara (Peru) described by De Iuliis *et al.* (2017) are considerably more sparse than those of *G. phoenesis* and *G. robustum*. Nevertheless, a small, worn nodular element, ROM 40613, was recovered from Talara and may represent an osteoderm or rudimentary phalanx. If this element is an osteoderm, it likely belongs to *G. tropicorum*, as there are no reliable reports (so far as we are able to ascertain) of the presence of osteoderms in the other two tardigrade clades present in the same fauna, the megatheriid *E. laurillardi* and scelidotheriine *Catonyx chiliense*; whereas they are not uncommon in Mylodontinae (see above).

Lund (1839) speculated on the role of osteoderms in the skin. He proposed that these mammals possessed a thick, roughened skin embedded with calcareous protrusions that gave it a nodular appearance, covered by a sparse coat of bristles. Lund (1950, p. 153) viewed these extinct mylodontoids as intermediate in appearance between living sloths and armadillos. In addition to enhanced protection due to the greater dermal consistency and toughness furnished by the ossicles, Cartelle & Bohórquez (1986) suggested two other possible functions for the osteoderms. One is that subcentral internal spaces within the osteoderms may have functioned as medullary cavities containing haematopoietic tissue. The other is that osteoderms may have played a role in thermoregulation. Nutrient foramina, related to vascular function, pierce one surface of an osteoderm, whereas the opposite surface is smooth and at times imperforate.

Conclusions

The analyses conducted in this report clearly support the erection of a new Pleistocene species of *Glossotherium* from the intertropical region of Brazil, *G. phoenesis*, represented in particular by a nearly complete skeleton and a second isolated skull. The numerous and clear morphological differences between this new species and the two others commonly recognized Pleistocene *Glossotherium* species were noted in the descriptions and comparisons.

We may thus recognize at least three Pleistocene species of *Glossotherium* species: *G. robustum*, *G. tropicorum* and *G. phoenesis* sp. nov. A fourth species of *Glossotherium*, *G. chapadmalensis* derives from the Pliocene of Argentina (Esteban 1996). Reconsideration of the validity of a fifth species, *G. tarijensis*, based on new specimens, is under study.

In addition to the already noted possible dimorphism in Megatheriidae and Scelidotheriinae, its presence among Mylodontinae is strengthened by the results of this contribution, reinforcing McDonald's (2006) proposal of dimorphism in *P. harlani*. The morphological evidence presented for *G. phoenesis*, particularly evident based on cranial remains, also lends support to the same proposal made over a century ago by Lydekker (1894) for *G. robustum*.

A detailed phylogenetic analysis based on 286 craniodental characters of 14 mylodontid taxa suggests

paraphyly of *Glossotherium* and close affinities between the recently revalidated *G. tropicorum* (De Iuliis *et al.* 2017) and *G. phoenesis*. However, given the age, size and paucity of remains of *Pleurolestodon*, and that our analysis employs only craniodental evidence, we consider it more prudent to refrain from upsetting the taxonomic cart until postcranial data may be included to allow more comprehensive phylogenetic studies. Such evidence is in the process of being recovered as part of the doctoral research of one of the authors (AB).

Acknowledgements

The authors thank C. de Muizon (MNHN) for providing images of *G. tropicorum*, K. L. Seymour (ROM) for allowing us to access specimens in his care, and B. Garzón (PUC Minas) for taking several of the photographs of the new *Glossotherium* species. We are grateful for the efforts of two anonymous reviewers, whose comments and suggestions greatly improved the manuscript.

Supplemental data

Supplementary material for this article can be found at: http://dx.doi.org/10.1080/14772019.2019.1574406

References

Abuhid, V. S. 1991. *Sobre um glossotério pleistocênico do Estado da Bahia, Brasil*. Unpublished MSc thesis, Instituto de Geociências da Universidade Federal do Rio de Janeiro, 136 pp.

Aguilera Socorro, O. A. 2006. *Tesoros paleontológicos de Venezuela: el cuaternario del Estado de Falcón*. Editorial Arte, Caracas, 120 pp.

Arzani, H., **Lanzelotto, S. L.**, **Suárez, G. E. A.** & **Novo, N. M.** 2014. Primer registro de pelos fósiles en *Glossotherium robustum* (Xenarthra, Mylodontidae), Pleistoceno tardío, Mercedes, Provincia de Buenos Aires, Argentina. *Ameghiniana*, **51**, 585–590. doi:10.5710/AMGH.20.10.2014.2798.

Bergqvist, L. P., **Gomide, M.**, **Cartelle, C.** & **Capilla R.** 1997. Faunas locais de mamíferos pleistocênicos de Itapipoca/Ceará, Taperoá/Paraíba e Campina Grande/Paraíba. Estudo comparativo, bioestratinômico e paleoambienta. *Geociências*, **2**, 23–32.

Bocquentin-Villanueva, J. 1979. *Mammiferes fossiles du Pléistocène Supérieur de Muaco, état de Falcon, Venezuela*. Unpublished PhD thesis, Université Pierre et Marie Curie, Paris, 112 pp, 31 pls.

Boscaini, A., **Iurino, D. A.**, **Billet, G.**, **Hautier, L.**, **Sardella, R.**, **Tirao, G.**, **Gaudin, T. J.** & **Pujos, F.** 2018. Phylogenetic and functional implications of the ear region anatomy of *Glossotherium robustum* (Xenarthra, Mylodontidae) from the Late Pleistocene of Argentina. *The Science of Nature*, **105**, 28. doi:10.1007/s00114-018-1548-y.

Boscaini, A., **Gaudin, T. J.**, **Mamani Quispe, B.**, **Münch, P.**, **Antoine, P.-O.** & **Pujos, F**. 2019. New well-preserved craniodental remains of *Simomylodon uccasamamensis* (Xenarthra, Mylodontidae) from the Pliocene of the Bolivian Altiplano: phylogenetic, chronostratigraphic, and paleobiogeographic implications. *Zoological Journal of the Linnean Society*, **185**, 459–89. doi:10.1093/zoolinnean/zly075.

Buckley, M., **Fariña, R. A.**, **Lawless, C.**, **Tambusso, P. S.**, **Varela, L.**, **Carlini, A. A.**, **Powell, J. E.** & **Martinez, J. G.** 2015. Collagen sequence analysis of the extinct giant ground sloths *Lestodon* and *Megatherium*. *PloS ONE*, **10**, e0144793. doi:10.1371/journal.pone.0139611.

Cabrera, A. 1936. Las especies del género "*Glossotherium*". *Notas del Museo de La Plata (Paleontología)*, **1**, 193–206.

Cartelle, C. 1994. Anomalias e desenvolvimento dentário em algumas espécies extintas de mamíferos do Brasil intertropical. *Acta Geologica Leopoldensia*, **17**, 573–584.

Cartelle, C. 2012. *Das grutas à luz: os mamíferos pleistocênicos de Minas Gerais*. Bicho do Mato, Belo Horizonte, 236 pp.

Cartelle, C. & **Bohórquez, G. A.** 1982. *Eremotherium laurillardi* (Lund, 1842). Parte I. Determinação específica e dimorfismo sexual. *Iheringia, Série Geológica*, **7**, 45–63.

Cartelle, C. & **Bohórquez, G. A.** 1986. Presença de ossículos dérmicos em *Eremotherium laurillardi* (Lund) Cartelle y Bohórquez, 1982. (Edentata, Megatheriidae). *Iheringia, Série Geológica*, **11**, 3–8.

Cartelle, C. & **De Iuliis, G.** 1995. *Eremotherium laurillardi*: the Panamerican late Pleistocene megatheriid sloth. *Journal of Vertebrate Paleontology*, **15**, 830–841. doi:10.1080/02724634.1995.10011265.

Cartelle, C. & **De Iuliis, G.** 2006. *Eremotherium laurillardi* (Lund) (Xenarthra, Megatheriidae), the Panamerican giant ground sloth: taxonomic aspects of the ontogeny of skull and dentition. *Journal of Systematic Palaeontology*, **4**, 199–209. doi:10.1017/S1477201905001781.

Cartelle, C. & **Fonseca, J. S.** 1981. Espécies do gênero *Glossotherium* no Brasil. *Anais do II Congresso Latino-Americano de Paleontologia*, **2**, 805–818.

Cartelle, C. & **Hiroka, S.** 2005. Primeiro registro pleistocênico de *Pteronura brasiliensis* (Gmelin, 1788) (Carnivora, Mustelidae). *Arquivos do Museu Nacional*, **63**, 595–598.

Cartelle, C., **Brant, W.** & **Piló, B.** 1989. A gruta do túnel de Santana (BA): morfogênese e paleontologia. *Anais do XI Congresso Brasileiro de Paleontologia*, **1**, 593–604.

Cartelle, C., **De Iuliis, G.** & **Pujos, F.** 2008. A new species of Megalonychidae (Mammalia, Xenarthra) from the Quaternary of Poço Azul (Bahia, Brazil). *Comptes Redus Palevol*, **7**, 335–346. doi:10.1016/j.crpv.2008.05.006.

Cartelle, C., **De Iuliis, G.** & **Ferreira, R. L.** 2009. Systematic revision of tropical Brazilian scelidotheriine sloths (Xenarthra, Mylodontoidea). *Journal of Vertebrate Paleontology*, **29**, 555–566. doi:10.1671/039.029.0231.

Cartelle, C. & **De Iuliis, G.** & **Pujos, F.** 2014. *Eremotherium laurillardi* (Lund, 1842) (Xenarthra, Megatheriinae) is the only valid megatheriine sloth species in the Pleistocene of intertropical Brazil: a response to Faure *et al.*, 2014.

Comptes Rendus Palevol, **14**, 15–23. doi:10.1016/j.crpv.2014.09.002.

Cope, E. D. 1889. The Edentata of North America. *American Naturalist*, **23**, 657–664.

Corona, A., **Perea, D.** & **McDonald, H. G.** 2013. *Catonyx cuvieri* (Xenarthra, Mylodontidae, Scelidotheriinae) from the late Pleistocene of Uruguay, with comments regarding the systematics of the subfamily. *Journal of Vertebrate Paleontology*, **33**, 1214–1225. doi:10.1080/02724634.2013.764311.

Dantas, M. A. T. 2009. Primeiro registro de fósseis de mamíferos pleistocênicos em caverna de Sergipe, Brasil. *Revista Brasileira de Paleontologia*, **12**, 161–164. doi:10.4072/rbp.2009.2.06.

Dechaseaux, C. 1971. *Oreomylodon wegneri*, édenté gravigrade du Pléistocène de l'Équateur: crâne et moulage endocrânien. *Annales de Paléontologie*, **57**, 243–285.

De Iuliis, G. & **Cartelle, C.** 1999. A new giant megatheriine ground sloth (Mammalia: Xenarthra: Megatheriidae) from the late Blancan to early Irvingtonian of Florida. *Zoological Journal of the Linnean Society*, **127**, 495–515. doi:10.1006/zjls.1998.0190.

De Iuliis, G., **Pujos, F.** & **Cartelle, C.** 2009. A new ground sloth (Mammalia: Xenarthra) from the Quaternary of Brazil. *Comptes Rendus Palevol*, **8**, 705–715. doi:10.1016/j.crpv.2009.07.003.

De Iuliis, G., **Pujos, F.**, **Toledo, N.**, **Bargo, M. S.** & **Vizcaíno, S. F.** 2014. *Eucholoeops* Ameghino, 1887 (Xenarthra, Tardigrada, Megalonychidae) from the Santa Cruz Formation, Argentine Patagonia: implications for the systematics of santacrucian sloths. *Geodiversitas*, **36**, 209–255. doi:10.5252/g2014n2a2.

De Iuliis, G., **Cartelle, C.**, **McDonald, H. G.** & **Pujos, F.** 2017. The mylodontine ground sloth *Glossotherium tropicorum* from the late Pleistocene of Ecuador and Peru. *Papers in Palaeontology*, **3**, 613–636. doi:10.1002/spp2.1088.

Delsuc, F., **Catzeflis, F. M**, **Stanhope, M. J.** & **Douzery, E. J. P.** 2001. The evolution of armadillos, anteaters and sloths depicted by nuclear and mitochondrial phylogenies: implications for the status of the enigmatic fossil *Eurotamandua*. *Proceedings of the Royal Society B*, **268**, 1605–1615. doi:10.1098/rspb.2001.1702.

Engelmann, G. F. 1985. The phylogeny of the Xenarthra. Pp. 51–64 in G. G. Montgommery (ed.) *The Ecology and Evolution of Armadillos, Sloths, and Vermilinguas*. Smithsonian Institution Press, Washington and London.

Esteban, G. I. 1996. *Revisión de los* Mylodontinae cuaternarios *(Edentata-Tardigrada) de Argentina, Bolivia y Uruguay. Sistemática, filogenia, paleobiología*, paleozoogeografía y paleoecología. Unpublished PhD thesis, Universidad Nacional de Tucumán, 336 pp.

Flower, W. H. 1883. On the arrangement of the orders and families of existing Mammalia. *Proceedings of the Zoological Society of London*, **51**, 178–186.

Gaudin, T. J. 2004. Phylogenetic relationships among sloths (Mammalia, Xenarthra, Tardigrada): the craniodental evidence. *Zoological Journal of the Linnean Society*, **140**, 255–305. doi:10.1111/j.1096-3642.2003.00100.x.

Gill, T. 1872. Arrangement of the families of mammals, with analytical tables. *Smithsonian Miscellaneous Collections*, **11**, 1–98.

Goloboff, P. A., **Farris, J. S.** & **Nixon K. C.** 2008a. TNT, a free program for phylogenetic analysis. *Cladistics*, **24**, 774–786. doi:10.1111/j.1096-0031.2008.00217.x.

Goloboff, P. A., **Farris, J. S.** & **Nixon K. C.** 2008b. *TNT: tree analysis using new technologies*. Program and documentation. Updated at http://www.zmuc.dk/public/phylogeny/TNT/

Haro, J. A., **Tauber, A. A.** & **Krapovickas, J. M.** 2016. The manus of *Mylodon darwinii* (Tardigrada, Mylodontidae) and its phylogenetic implications. *Journal of Vertebrate Paleontology*, **36**, e1188824. doi:10.1080/02724634.2016.1188824.

Hautier, L., **Billet, G.**, **Eastwood, B.** & **Lane, J.** 2014. Patterns of morphological variation of extant sloth skulls and their implication for future conservation efforts. *The Anatomical Record*, **297**, 979–1008. doi:10.1002/ar.22916.

Henriques, D. D. R. 1992. *Os fósseis de Lestodon Gervais, 1855 (Edentata, Mylodontidae) da coleção de Paleovertebrados do Museu Nacional/UFRJ. Estudo morfológico e comparativo*. Unpublished MSc thesis, Universidade Federal do Rio de Janeiro, 182 pp.

Hill, R. V. 2006. Comparative anatomy and histology of xenarthran osteoderms. *Journal of Morphology*, **267**, 1441–1460. doi:10.1002/jmor.10490.

Hoffstetter, R. 1948. Nota preliminar sobre los Edentata Xenarthra del Pleistoceno Ecuatoriano. II: Mylodontidae. *Boletín de Informaciones Científicas Nacionales de Quito*, **2**, 19–42.

Hoffstetter, R. 1949. Nuevas observaciones sobre los Edentata del Pleistoceno superior de la Sierra ecuatoriana. *Boletín de Informaciones Científicas Nacionales de Quito*, **3**, 67–99.

Hoffstetter, R. 1952. Les mammifères pléistocènes de la République de l'Équateur. *Mémoires de la Société Géologique de France*, **66**, 1–391.

Hoffstetter, R. 1956. Contribution à l'étude des Orophodontoidea, Gravigrades cuirassés de la Patagonie. *Annales de Paléontologie*, **42**, 27–64.

Hoffstetter, R. 1959. Généralité d'une circulation veineuse intrarachidienne chez les Édentés Tardigrades (Paresseux et Gravigrades). *Bulletin du Muséum National d'Histoire Naturelle*, **31**, 181–187.

Lara-Ruiz, P. & **Chiarello, A. G.** 2005. Life-history traits and sexual dimorphism of the Atlantic forest maned sloth *Bradypus torquatus* (Xenarthra: Bradypodidae). *Journal of Zoology*, **267**, 63–73. doi:10.1017/S0952836905007259.

Lund, P. W. 1839. Blik paa Brasiliens Dyreverden för Sidste Jordomvaeltning. Anden Afhandling: Pattedyrene. *Det Kongelige Danske Videnskabernes Selskbas Naturvidenskabelige og Mathematiske Afhandlinger*, **8**, 61–144.

Lund, P. W. 1846. Meddelelse af Det Udbytte de i 1844 undersögte knoglehuler have afgivet til hundskaben om Brasiliens dyreverden för sidste jordomvaeltning. *Det Kongelige Danske Videnskabernes Selskbas Naturvidenskabelige og Mathematiske Afhandlinger*, **12**, 1–94.

Lund, P. W. 1950. *Memórias sôbre a paleontologia Brasileira. Revistas e comentadas por Carlos de Paula Couto*. Ministério de Educaçao e Saude, Instituto Nacional do Livro, Rio de Janeiro, 589 pp.

Lydekker, R. 1894. Contributions to a knowledge of the fossil vertebrates of Argentina. 2. The extinct edentates of

Argentina. *Anales del Museo de La Plata (Paleontología)*, **3**, 1–118.

Maddison, W. P. & **Maddison D. R.** 2011. Mesquite: a modular system for evolutionary analysis. Version 2.75. Available at http://mesquiteproject.org

Martin, F. M. 2018. Cueva del Milodón. The hunting grounds of the Patagonia panther. *Quaternary International*, **466**, 212–222. doi:10.1016/j.quaint.2016.05.005.

McAfee, R. K. 2009. Reassessment of the cranial characters of *Glossotherium* and *Paramylodon* (Mammalia: Xenarthra: Mylodontidae). *Zoological Journal of the Linnean Society*, **155**, 885–903. doi:10.1111/j.1096-3642.2008.00468.x.

McDonald, H. G. 2006. Sexual dimorphism in the skull of Harlan's ground sloth. *Contributions in Science*, **510**, 1–9.

McDonald, H. G. 2018. An overview of the presence of osteoderms in sloths: implications for osteoderms as a plesiomorphic character of the Xenarthra. *Journal of Mammalian Evolution*, **24**, 485–493. doi:10.1007/s10914-017-9415-8.

McDonald, H. G. & **De Iuliis, G.** 2008. Fossil history of sloths. Pp. 39–55 in S. F. Vizcaíno & W. J. Loughry (eds) *The biology of the Xenarthra*. University Press of Florida, Gainesville.

Merriam, J. C. 1906. Recent discoveries of Quaternary mammals in Southern California. *Science*, **24**, 248–250.

Miño-Boilini, A. R. & **Zurita, A. E.** 2015. Dimorphism in Quaternary Scelidotheriinae (Mammalia, Xenarthra, Phyllophaga). *Paleontologia Electronica*, **18**(1), 12A. doi.org/10.26879/434.

Mones, A. 1986. Palaeovertebrata sudamericana. Catálogo sistemático de los vertebrados fósiles de América del Sur. Parte I. Lista preliminar y bibliografía. *Courier Forschungsinstitut Senckenberg*, **82**, 1–625.

Montellano-Ballesteros, M. & **Carranza-Castañeda, Ó.** 1986. Descripción de un milodóntido del Blancano temprano de la mesa central de México. *Revista del Instituto de Geología de la Universidad Nacional Autónoma de México*, **6**, 193–203.

Moreno, P. & **Woodward, A. S.** 1899. On a portion of mammalian skin, named *Neomylodon listai*, from a cavern near Consuelo Cove, Last Hope Inlet, Patagonia, with a description of the specimen. *Proceedings of the Zoological Society of London*, 144–156.

Morgan, G. S. 2008. Vertebrate fauna and geochronology of the Great American Biotic Interchange in North America. *New Mexico Museum of Natural History and Science*, **44**, 93–140.

Naples, V. L. 1982. Cranial osteology and function in the tree sloths, *Bradypus* and *Choloepus*. *American Museum Novitates*, **2739**, 1–41.

Naples, V. L. 1990. Morphological changes in the facial region and a model of a dental growth and wear pattern development in *Nothrotheriops shastensis*. *Journal of Vertebrate Paleontology*, **10**, 372–389.

Negri, F. R., **Bocquentin-Villanueva, J.**, **Ferigolo, J.** & **Antoine, P.-O.** 2010. A review of Tertiary mammal faunas and birds from western Amazonia. Pp. 243–258 in C. Horn & F. P. Wesselingh (eds) *Amazonia, landscape and species evolution: a look into the past*. Blackwell-Wiley, Hoboken.

Owen, R. 1839. Fossil Mammalia (3). Pp. 65–80 in C. Darwin (ed.) *The zoology of the voyage of H.M.S. Beagle, under the command of Captain Fitzroy, during the years 1832 to 1836*. Smith, Elder & Co., London.

Owen, R. 1842. *Description of the skeleton of an extinct gigantic sloth*, Mylodon robustus*, Owen, with observations on the osteology, natural affinities, and probable habits of the megatherioid quadrupeds in general*. Royal College of Surgeons of England, London, 176 pp.

Patterson, B., **Turnbull, W. D.**, **Segall, W.** & **Gaudin, T. J.** 1992. The ear region in Xenarthrans (=Edentata: Mammalia). Part II. Pilosa (Sloths, Anteaters), Palaeanodonts, and a Miscellany. *Fieldiana*, **24**, 1–78. doi:10.5962/bhl.title.3466.

Paula-Couto, C. de 1953. *Paleontologia Brasileira. Mamíferos*. Biblioteca Científica Brasileira, Instituto Nacional do Livro, 516 pp.

Pitana, V. G., **Esteban, G. I.**, **Ribeiro, A. M.** & **Cartelle, C.** 2013. Cranial and dental studies of *Glossotherium robustum* (Owen, 1842) (Xenarthra: Pilosa: Mylodontidae) from the Pleistocene of southern Brazil. *Alcheringa*, **37**, 147–162. doi:10.1080/03115518.2012.717463.

Politis, G. G. & **Messineo, P. G.** 2008. The Campo Laborde site: new evidence for the Holocene survival of Pleistocene megafauna in the Argentine Pampas. *Quaternary International*, **191**, 98–114. doi:10.1016/j.quaint.2007.12.003.

Prothero, D. & **Raymond, K.** 2008. Variation and sexual size dimorphism in Pleistocene ground sloths (Xenarthra). *New Mexico Museum of Natural History and Science Bulletin*, **44**, 331–333.

Pujos, F., **De Iuliis, G.** & **Cartelle, C.** 2017. A paleogeographic overview of tropical fossil sloths: towards an understanding of the origin of extant suspensory sloths? *Journal of Mammalian Evolution*, **24**, 19–38. doi:10.1007/s10914-016-9330-4.

Rinderknecht, A., **Bostelmann, E.**, **Perea, D.** & **Lecuona, G.** 2010. A new genus and species of Mylodontidae (Mammalia: Xenarthra) from the late Miocene of southern Uruguay, with comments on the systematics of the Mylodontinae. *Journal of Vertebrate Paleontology*, **30**, 899–910. doi:10.1080/02724631003757997.

Rovereto, C. 1914. Los estratos Araucanos y sus fósiles. *Anales del Museo Nacional de Historia Natural de Buenos Aires*, **25**, 1–250.

Saint-André, P.-A., **Pujos, F.**, **Cartelle, C.**, **De Iuliis, G.**, **Gaudin, T. J.**, **McDonald, H. G.** & **Mamani Quispe, B.** 2010. Nouveaux paresseux terrestres (Mammalia, Xenarthra, Mylodontidae) du Néogène de l'Altiplano bolivien. *Geodiversitas*, **32**, 255–306. doi:10.5252/g2010n2a4.

Salles, L. O., **Cartelle, C.**, **Guedes, P. G.**, **Boggiani, P. C.**, **Janoo, A.** & **Russo, C. A. M.** 2006. Quaternary mammals from Serra da Bodoquena, Mato Grosso do Sul, Brazil. *Boletim do Museu Nacional, Nova Série Zoologia*, **521**, 1–12.

Silva, D. D. & **Sedor, F. A.** 2008. Mamíferos pleistocênicos do estado do Paraná, Brasil. *Anais da III Congreso Latino Americano de Paleontología de Vertebrados*, **1**, 234.

Simpson, G. G. & **Paula-Couto, C. de** 1981. Fossil mammals from the Cenozoic of Acre, Brazil, III. Pleistocene Edentata Pilosa, Proboscidea, Sirenia, Perissodactyla and Artiodactyla. *Iheringia, Série Geologia*, **6**, 11–73.

Sinclair, W. J. 1910. Dermal bones of *Paramylodon* from the asphaltum deposits of Rancho La Brea, near Los Angeles,

California. *Proceedings of the American Philosophical Society*, **49**, 191–195.

Slater, G., **Cui, P.**, **Forasiepi, A. M.**, **Lenz, D.**, **Tsangaras, K.**, **Voirin, B.**, **Moraes, N.**, **MacPhee, R. D. E.** & **Greenwood, A. D.** 2016. Evolutionary relationships among extinct and extant sloths: the evidence of metagenomes and retroviruses. *Genome Biology and Evolution*, **80**, 607–621. doi:10.1093/gbe/evw023.

Spillmann, F. 1931. *Die Säugetiere Ecuadors im Wandel der Zeit*. Universidad Central, Quito, 112 pp.

Stock, C. 1925. Cenozoic gravigrade edentates of western North America with special reference to the Pleistocene Megalonychidae and Mylodontidae of Rancho La Brea. *Publications of the Carnegie Institution of Washington*, **331**, 1–206.

Toledo, P. M. 1986. *Descrição do sincrânio de Eremotherium laurillardi Lund, 1842, taxonomia e paleobiogeografia*. Unpublished MSc thesis, Universidade Federal do Rio Grande do Sul, Porto Alegre, 127 pp.

Vialou, A. V., **Aubry, T.**, **Benabdelhadi, M.**, **Cartelle, C.**, **Figuti, L.**, **Fontugne, M.**, **Solari, M. E.** & **Vialou, D.** 1995. Découverte de Mylodontinae dans un habitat préhistorique daté du Mato Grosso (Brésil): l'abri rupestre de Santa Elina. *Comptes Rendus de l'Académie des Sciences de Paris*, **320**, 655–661.

Winge, H. 1915. Jordfundne og nulevende gumlere (Edentata) fra Lagoa Santa, Minas Gerais, Brasilien: med udsigt over gumlernes indbyrdes slaegtskab. *E Museo Lundii*, **3**, 1–321.

Ximenes, C. L., **Santos A. S. T.** & **Monteiro, F. A. C.** 2010. Nota preliminar sobre os fósseis de vertebrados do sítio paleontológico do Jirau, Pleistoceno de Itapipoca, estado do Ceará. *Anais da Simpósio Brasileiro de Paleontologia de Vertebrados*, **1**, 122.

Associate Editor: Pip Brewer